NASA Contractor Report 3685

A Theory of Rotating Stall of Multistage Axial Compressors

F. K. Moore

INTERGOVERNMENTAL PERSONNEL AGREEMENT 810-626-1
JULY 1983

25th Anniversary
1958-1983

NASA

NASA Contractor Report 3685

A Theory of Rotating Stall of Multistage Axial Compressors

F. K. Moore
Cornell University
Ithaca, New York

Prepared for
Lewis Research Center
under Intergovernmental Personnel Agreement 810-626-1

National Aeronautics
and Space Administration

**Scientific and Technical
Information Branch**

1983

FOREWORD

The research described in this report was performed at Lewis Research Center during the period August 1981 to August 1982, while the author was the Addison P. Rothrock Visiting Scientist at Lewis, on sabbatic leave from Cornell University. The work was done in the Fan and Compressor Branch of the Fluid Mechanics and Acoustics Division, in support of their program of research on non-recoverable stall of axial compressors.

L. Reid and M. E. Goldstein of Lewis and Prof. E. M. Greitzer of MIT provided helpful suggestions concerning this effort.

TABLE OF CONTENTS

PART I - SMALL DISTURBANCES

SUMMARY

An analysis is made of rotating stall in compressors of many stages, finding conditions under which a flow distortion can occur which is steady in a traveling reference frame, even though upstream total and downstream static pressure are constant. In the compressor, a pressure-rise hysteresis is assumed. Flow in entrance and exit ducts yield additional lags. These lags balance to give a formula for stall propagation speed. For small disturbances, it is required that the compressor characteristic be flat in the neighborhood of average flow coefficient.

Results are compared with the experiments of Day and Cumpsty. If a compressor lag of about twice that due only to fluid inertia is used, predicted propagation speeds agree almost exactly with experimental values, taking into account changes of number of stages, stagger angle, row spacing, and number of stall zones. The agreement obtained gives encouragement for the extension of the theory to account for large amplitudes.

INTRODUCTION

In recent years experimental studies and reviews by Greitzer, Day and Cumpsty (1,2,3) have clarified and redefined the problem of rotating stall of axial flow compressors, giving a new emphasis to the compressor of many stages. At low flows, virtually all compressors exhibit zones of stalled flow which propagate tangentially, with blade passages cyclically stalling and recovering in the manner first described by Emmons (4).

However, when the compressor has many stages (about three seems to suffice), the stall patterns seem to be simpler and presumably more predictable than when the compressor consists of a single row or stage. Early reviews (5) convey this impression, but it remained for Day, Greitzer and Cumpsty (3) to describe what one might call the kinematics of rotating stall. They demonstrated, for example, that the stall pattern in "deep stall" tends to run straight through the machine, with an especially abrupt transition at the trailing edge of the stall zone.

Theoretical studies in the past (6,7,8) have attempted to understand rotating stall for a single stage under the natural impression that if one could properly relate the Emmons type of stalling-unstalling episodes to the individual cascade characteristics, then one could proceed to synthesize a theory for multistage machines. This approach, though logical, has not been fruitful. In effect, rotating stall is too universal a phenomenon and depends on too many variables; single-stage analysis does not yield critical conditions meaningful for whole-compressor performance, especially in deep stall.

In the present three-part study, we explore the idea that rotating stall theory should begin with the compressor of many stages, operating in stall. Doing this, we will not emphasize the problem of "stall inception," but, rather, try to incorporate in the theory the kinematic features of deep stall described by Day, Cumpsty and Greitzer (3). Greitzer and Cumpsty (9) have presented a semi-empirical analysis of deep-stall propagation speed which is in this same spirit.

In Part I, a single dynamic hysteresis is assumed for the blade-passage force function and conditions are derived for the occurrence of a weak stall pattern which is steady in some rotating frame of reference. From this analysis we find a formula for stall propagation speed which agrees well with experimental data, if the single lag parameter is properly chosen.

In Part II, the analysis is extended to describe the stall patterns of arbitrary velocity amplitude which can occur when the quasi-steady compressor characteristic is either flat (deep stall) or else curved as it would be at stall inception. Wave forms for velocities and pressure are found, as well as propagation speeds and the distortion of the compressor characteristic due to rotating stall.

In Part III, a compressor characteristic is adopted which has the realistic feature of an unstalled region with peak pressure rise, a deep-stall valley, and a steep resistance to reversed flow. Rotating stall then is found to have the nature of a limit cycle, familiar in the classical van der Pol problem of nonlinear mechanics (10). Results include a prediction of stall recovery as flow coefficient is increased.

The present Part I, though limited in results to weak disturbances, will include certain developments in forms suitable for more general application in the subsequent parts.

Notation is defined, for all three parts, in Appendix F.

THE COMPRESSOR

The compressor is assumed to have a constant-speed characteristic as sketched in the solid line of Fig. 1.1. We will denote the upstream total (p_T) to downstream static (p_S) pressure-rise coefficient by ψ_c, in the absence of rotating stall:

$$\frac{p_S - p_T}{\rho U^2} \equiv \psi_c(\phi). \tag{1.1}$$

The axial flow coefficient ϕ has the average value Φ:

$$\frac{v}{U} \equiv \phi; \quad \frac{V}{U} \equiv \Phi. \tag{1.2}$$

The characteristic ψ_c will be considered to be single-valued, as shown. Throttle settings, indicated by dashed parabolic lines, will intersect the characteristic and establish operating points (A-E on the sketch) about which rotating stall might occur. Points B and D in the sketch would indicate limits of a quasi-steady hysteresis loop (B-C-D-E) due (we assume) purely to the way the throttle parabolas intersect the characteristic. In parts II and III, we shall permit the net pressure rise (Ψ) to depend on the existence of rotating stall. For example, the operating point in rotating stall for the Φ indicated at point A might actually lie above or below the characteristic curve.

The compressor has N stages, with IGV and OGV rows providing zero incidence at design. Blading and design vector diagrams are symmetrical (50% reaction) as sketched in Fig. 1.2. Radial effects will be neglected, and flows will be considered incompressible.

FLOW DISTURBANCE IN THE COMPRESSOR

First, a disturbance will be postulated to exist in the compressor, steady in a circumferentially moving frame. This disturbance implies disturbances in the flow fields entering and leaving the compressor. The plan of this study is to find the requirement that such a set of disturbances exists, even though pressures far upstream and downstream remain constant; in effect, to find eigensolutions and eigenvalues for the whole system. We begin by describing the disturbance of a single blade passage.

Disturbance in a Blade Passage

When rotating stall occurs, flow velocities will change locally and in time. We will assume that when axial flow is slowly reduced, keeping U constant, flow fields of rotor and stators remain symmetrical, though pressure rise and deviation should change. In other words, the quasi-steady velocity triangles remain symmetrical, and corresponding pressure changes are equal. Pressure rise in each row is assumed to depart slightly from the quasi-steady, however.

The static pressure rise through each row will be assumed to have the form

$$\frac{\Delta p}{\frac{1}{2}\rho U^2} = F(\phi) - \tau(\phi)\dot{\phi} \tag{1.3}$$

whether rotor or stator.

The quasi-steady pressure-rise coefficient F might have the form sketched in Fig. 1.3. Assigning the same F to each row, and properly taking account of dynamic pressure, $F(\phi)$ will yield the ψ_c of Fig. 1.1. The occurrence of a maximum of F, and the drop of F as ϕ is reduced, will signify stall of a blade passage.

The second term describes hysteresis due either to flow acceleration, flow separation or viscous processes in the blade passage. It is written in the sense that if ϕ is decreasing, then there is an extra force which is positive. At any flow coefficient, therefore, we assume a counter-clockwise dynamic hysteresis loop, as sketched in Fig. 1.4. The parameter τ will generally be a function of ϕ, of course. However, throughout this study, we will take τ to be constant, and the same for rotors and stators.

Because Eq. (1.3) will be considered to apply equally to the rotor and stator rows, in effect we disregard centrifugal and secondary-flow phenomena. In fact, for symmetric blading, τ would be the same for rotors and stators. For guide vanes, we will adopt the same equation, using subscripts to distinguish them from the stage elements.

Stall Pattern of the Compressor

If, by symmetry, rotor and stator blade passages show no deviation under disturbance, and no flow development takes place between rows (as if there is zero inter-row spacing), then continuity will require that all instantaneously-connected blade passages have the same axial velocity. Therefore, any disturbance of axial velocity would be purely circumferential, however many stages there are, and whatever the speed of propagation of the disturbance pattern. Further study might show that dynamic effects will require modification of this symmetry argument.

Under present assumptions, a stall pattern, shown shaded on Fig. 1.4, must proceed straight through the machine. This is consistent with observations of deep stall. Obviously, if reaction is not 50% or blades are of unequal axial length, if compressibility or centrifugal effects were significant, or if circumferential flow between rows is allowed, then the straight-through pattern would not be correct.

Next we assume that a disturbance pattern is steady in some rotating frame of reference. If the compressor is "unwrapped" as in Fig. 1.4, the disturbance is moving to the right with speed fU relative to stators. The "stall propagation speed" f is unknown; it is to be found as an eigenvalue of the disturbance, so to speak. Relative to the disturbance, stators are moving to the left with speed fU and rotors are therefore moving to the right with speed (1-f)U. The axial flow coefficient, in this frame, takes the form

$$\phi = \Phi + g(\theta) \qquad (1.4)$$

where g represents a steady disturbance. Again referring to Fig. 1.4, distance x is measured to the right, so that

$$\theta = 2x/D \tag{1.5}$$

where D is the mean diameter of the compressor. If the disturbance of ϕ is purely circumferential, then Eq. (1.3) applies equally to each blade row, and pressure-rise may be accumulated through the compressor purely as a function of θ, or equivalently, x.

The time derivative $\dot{\phi}$ must be expressed in terms of the steady disturbance described in Eq. (1.4) and Fig. 1.4; it signifies the rate of increase of ϕ experienced by a blade passage as it traverses the postulated stall disturbance. Thus, from Eqs. (1.4) and (1.5),

$$\dot{\phi} = g'(\theta)\dot{\theta} = g'(\theta)\,\frac{2\dot{x}}{D}\,. \tag{1.6}$$

Fig. 1.4 sketches the situation: The solid line represents the steady but disturbed flow, $\phi(\theta)$. Stator blades moving the the left at speed fU experience an increase of ϕ depending on the local gradient of ϕ (that, is, $\phi'(\theta)$) and the relative speed $\dot{x} = -fU$. Similarly, a rotor moves in the same gradient with speed $\dot{x} = (1-f)U$. For stators and rotors separately,

$$\dot{\phi}_{stator} = -g'(\theta)\,\frac{2U}{D}\,f \tag{1.7a}$$

$$\dot{\phi}_{rotor} = g'(\theta)\,\frac{2U}{D}\,(1-f). \tag{1.7b}$$

Since it is intended to accumulate forces through the compressor, we will find use for the combined pressure-rise expression for a single stage:

$$\left(\frac{\Delta p}{\frac{1}{2}\rho U^2}\right)_{stage} = 2F(\phi) - \tau g'(\theta)\,\frac{4U}{D}\,(\tfrac{1}{2} - f)\,. \tag{1.8}$$

Guide Vanes

The OGV is assumed to have no deviation, and will therefore deliver flow in a purely axial direction to the diffuser. A hysteresis term (Eq. (1.3)) applies, with a value of τ_{OV} presumably different from the τ applicable to stators and rotors of the stages.

It will be assumed that IGV's are purely axial at entrance. When rotating stall occurs, there will be (as we shall find) a transverse velocity disturbance at the compressor (IGV) entrance. In this paper, we will consider this velocity disturbance small compared to V. Regarding the IGV as a nozzle, its entering velocity will therefore depart from the local value of v only to second order in small quantities.

Accordingly, although there must be a rather abrupt pressure rise crossing the entrance plane of the IGV's, it too will be of second order in flow deflection. By our previous stage symmetry argument, we should expect the IGV discharge angle to be the same as the OGV entrance angle. Thus, recalling Eq. (1.3), there should be a negative value of F for the IGV nozzle, just equal to the positive value for the OGV passage acting as a diffuser, even though ϕ varies. Again a hysteresis term should apply, and, for OGV and IGV together, one has, corresponding to Eq. (1.8),

$$\left(\frac{\Delta p}{\frac{1}{2}\rho U^2}\right)_{\substack{\text{guide}\\ \text{vanes}}} = (\tau_{IV} + \tau_{OV})g'(\theta)\,\frac{2U}{D}\,f + K_I h^2 \tag{1.9}$$

where $K_I h^2$ represents the coefficient of abrupt pressure rise at the IGV entrance.

UPSTREAM DISTURBANCE

Far upstream, we imagine a reservoir of total pressure p_T, constant whether or not rotating stall is progress. Between that reservoir and the compressor face is a flow passage of some possibly complex shape ("Gooseneck"). In that region, a flow disturbance will develop, if rotating stall exists. In this study, we shall assume the entrance region to be a straight, uniform channel. In that case, if the flow upstream has uniform velocity and pressure,

$$p_\infty = p_T - \frac{1}{2}\rho V^2 \tag{1.10}$$

and V will be the average velocity of any disturbance that arises downstream.

Velocity Field

In the channel, disturbances will be considered irrotational as well as incompressible. Thus, Laplace's equation applies. For convenience, we adopt the coordinate system of Fig. 1.4, so that the velocity components far upstream ($y = -\infty$) are

$$\frac{u_\infty}{U} = -f; \quad \frac{v_\infty}{U} = \frac{V}{U} \equiv \Phi. \tag{1.11}$$

At the compressor face, Eq. (1.4) applies:

$$\frac{v}{U} = \phi = \Phi + g(x). \tag{1.12}$$

The resulting steady streamline pattern in the entrance duct region will be as sketched in Fig. 1.5. It will be necessary to know the pressure disturbance at the compressor face, and for this, the value of u there is needed. We may write a disturbance velocity potential

$$\frac{u}{U} = -f + \tilde{\phi}_x; \quad \frac{v}{U} = \Phi + \tilde{\phi}_y \tag{1.13}$$

with $\tilde{\phi}$ vanishing when $y = -\infty$, and at $y = 0$,

$$(\tilde{\phi}_y)_o = g(\theta) \tag{1.14}$$

where g is arbitrary but periodic, with wave length $\pi D/n$. The wave number n is introduced to account for the possibility of multiple-cell stall. The required u-velocity at the compressor face will henceforth be designated as h(x):

$$(\tilde{\phi}_x)_o = h(\theta). \tag{1.15}$$

In general, h is the Hilbert transform of g:

$$h(\theta) = -\frac{1}{\pi} \int_{-\infty}^{\infty} \frac{g(\xi)d\xi}{\theta - \xi} . \tag{1.16}$$

If g is periodic, it may be shown that Eq. (1.16) yields

$$h = -\frac{1}{\pi} \int_0^{2\pi} g'(\xi) \ln\left|\sin \frac{\theta-\xi}{2}\right| d\xi. \tag{1.17}$$

If $g(\theta)$ has a Fourier series,

$$g(\theta) = \sum_1^{\infty} (a_n \sin n\theta + b_n \cos n\theta) \tag{1.18a}$$

then

$$\tilde{\phi}(y,\theta) = \sum_1^{\infty} \frac{D}{2n} e^{n\frac{2y}{D}} (a_n \sin n\theta + b_n \cos n\theta) \tag{1.18b}$$

which satisfies Eq. (1.14) and vanishes at $y = -\infty$. The corresponding u and v velocities both vanish as they should at $y = -\infty$, and

$$h(\theta) = \sum_1^{\infty} (a_n \cos n\theta - b_n \sin n\theta). \tag{1.18c}$$

For example, if g is a harmonic wave,

$$g = \varepsilon\Phi \sin n\theta; \quad h = \varepsilon\Phi \cos n\theta, \tag{1.19}$$

ε being an amplitude parameter.

Pressure Field

In the disturbance coordinates, the steady Bernoulli equation applies:

$$p_\infty + \frac{1}{2}\rho U^2(f^2+\Phi^2) = p_o + \frac{1}{2}\rho U^2[(-f+h)^2+(\Phi+g)^2] \tag{1.20}$$

where p_o is the pressure at the compressor face, just ahead of the IGV. Recalling Eq. (1.10), one finds

$$\frac{p_o-p_T}{\rho U^2} = -(\frac{1}{2}\Phi^2 + \Phi g + \frac{1}{2}g^2 - fh + \frac{1}{2}h^2). \tag{1.21}$$

If g is a weak harmonic wave, Eq. (1.19), with ε assumed small compared to 1, would provide

$$\frac{p_o-p_T}{\rho U^2} = -\frac{1}{2}\Phi^2 - \varepsilon(\Phi^2 \sin n\theta - f\Phi \cos n\theta) \tag{1.22}$$

to first order in ε.

If the channel is not straight, or if the flow in the channel is not irrotational, Eqs. (1.21) and (1.22) would require modification.

DOWNSTREAM DISTURBANCE

Far downstream, we imagine a flow of uniform static pressure (p_s), but not necessarily constant velocity; a shear flow might be the final result. The flow is expected to emerge from the OGV in an axial direction (viewed in stator coordinates) but with varying pressure (p_e) and perhaps vorticity. The actual exit-flow device, or diffuser, is very important in this regard, and we will limit this discussion to two types, a straight channel, and a sudden expansion. These two extreme types perhaps bracket the possibilities.

Straight Channel

If there is a straight, constant-area channel downstream of the compressor exit (Fig. 1.6a) then the Euler equations must be solved in the region sketched in Fig. 1.5. Defining a stream function for that region,

$$\frac{u}{U} = \tilde{\psi}_y; \quad \frac{v}{U} = \phi = -\tilde{\psi}_x \tag{1.23}$$

and expressing pressure in the dimensionless form

$$\frac{p_s - p}{\rho U^2} \equiv P \tag{1.24}$$

where p_s is the (constant) downstream static pressure, one may write the Euler equations as

$$-P_x = -\tilde{\psi}_y\tilde{\psi}_{xy} + \tilde{\psi}_x\tilde{\psi}_{yy}; \quad -P_y = \tilde{\psi}_y\tilde{\psi}_{xx} - \tilde{\psi}_x\tilde{\psi}_{xy}. \tag{1.25}$$

Boundary conditions at the rear face of the compressor (subscript e) at y = 0 are

$$(\tilde{\psi}_y)_e = -f; \quad -(\tilde{\psi}_x)_e = \Phi + g(x) \tag{1.26}$$

and far downstream (subscript s) at $y = \infty$, the pressure must become uniform, but vortical velocity disturbances may survive:

$$P_s = 0. \tag{1.27}$$

In formulating a solution of the system of Eqs. (1.25-27), we should recall that only P is needed, in its relation to the disturbance function g(x). Eq. (1.25) can be converted to

$$\frac{1}{2}\nabla^2 P = -\tilde{\psi}_{xx}\tilde{\psi}_{yy} + (\tilde{\psi}_{xy})^2 \tag{1.28}$$

and Eqs. (1.25) and (1.26) yield

$$(P_y)_e = -fg'(x). \tag{1.29}$$

Of course, one or the other of Eq. (1.25) must be included with Eq. (1.28). However, if the disturbance is weak, then the right side of Eq. (1.28) is of second order, and Eq. (1.28) is simply Laplace's equation

$$\nabla^2 P = 0. \tag{1.30}$$

The desired solution for P can be found directly, using Eqs. (1.27) and (1.29) as boundary conditions.

In fact, the function -P/f would correspond to the x-derivative of a velocity potential, vanishing at $y = \infty$, of which g(x) is the y-derivative at y = 0. But that is precisely the relationship between g and h defined in Eqs. (1.14) and (1.15). Taking account of the difference of direction of y between the two cases, one may immediately conclude that

$$P_e = fh; \quad P_e \equiv \frac{p_s - p_e}{\rho U^2}. \tag{1.31}$$

This is not a general result, because the right side of Eq. (1.28) was set equal to zero. It is, however, correct to first order in small quantities if, for example, Eq. (1.19) applies, and may be a useful relation even if disturbances are not weak.

If disturbances are indeed weak, Eqs. (1.25) and (1.31) may be used to find the velocity field in the straight channel. The result for $\tilde{\psi}$ is

$$\begin{aligned}\tilde{\psi} = \frac{D}{2n} \{ & -\Phi n(\theta + 2\frac{f}{\Phi}\frac{y}{D}) + \\ & \varepsilon \frac{\Phi^2}{\Phi^2+f^2} [f \sin n(\theta + 2\frac{f}{\Phi}\frac{y}{D}) \\ & + \Phi \cos n(\theta + 2\frac{f}{\Phi}\frac{y}{D}) \\ & + \frac{f}{\Phi} e^{-2n\frac{y}{D}} (-\Phi \sin n\theta + f \cos n\theta)]\}.\end{aligned} \tag{1.32}$$

If disturbances are of finite strength, and if $g(\theta)$ can be expressed as a Taylor series in ε, then the full Eq. (1.28) could be made the basis of a method of successive approximations.

Sudden Expansion

If there is a sudden large transverse (radial) expansion just at the OGV exit, as sketched in Fig. 1.6b, then the exit flow would be like a jet emerging from a long slot. While the jet velocity would vary circumferentially on a scale comparable to wheel diameter, the

pressure matching of the jet to the receiver would occur on the scale of blade height. Since the receiver pressure could be considered constant, the jet exit pressure could also be considered constant. In this extreme of an orifice-like diffuser,

$$p_e = p_s. \tag{1.33}$$

This is the simplest possible assumption about pressure change at the compressor exit. Of course, it envisages an extremely short diffuser, which would generally not be acceptable because of its low efficiency.

Apparently, the general problem of finding the pressure change at the compressor exit is quite difficult, both to define and to solve. The specifics of diffuser configuration would greatly affect the result. Here, we have found expressions for two extreme cases which may possibly bracket typical practical situations. We may, for convenicence, write them in the form

$$P_e = \frac{p_s - p_e}{\rho U^2} = (m-1)fh \tag{1.34}$$

where m = 1 would signify a sudden area change, and m = 2 would signify a straight channel. We will regard m, therefore, as a somewhat arbitrary parameter of our problem.

REQUIREMENTS FOR ROTATING STALL

The various pressure relations may now be combined to express a statement that pressures remain constant in upstream and downstream reservoirs, even though an unsteady disturbance occurs in the compressor which connects them. We have already specified that the disturbance is steady when viewed in a frame rotating with velocity fU.

Pressure Match

We require that $p_s - p_T$ be constant, or

$$\underbrace{\frac{p_o - p_T}{\rho U^2}}_{\text{entrance duct}} + \underbrace{\frac{p_e - p_o}{\rho U^2}}_{\text{compressor}} + \underbrace{\frac{p_s - p_e}{\rho U^2}}_{\text{exit duct}} = \underbrace{\frac{p_s - p_T}{\rho U^2}}_{\text{reservoirs}} \equiv \Psi. \tag{1.35}$$

The first term is given by Eq. (1.21), the third by Eq. (1.34), and the second by application of Eq. (1.9) for guide vanes and Eq. (1.8) for each of N stages. The result may be written

$$[\frac{2UN\tau}{D}\ (\frac{1}{2} - f) - \frac{U(\tau_{IV}+\tau_{OV})}{D}\ f]g'(\theta) - mfh + \frac{1}{2}\ h^2$$

$$- \frac{1}{2}\ K_I h^2 + \Psi - [NF(\phi) - \frac{1}{2}\ \phi^2] = 0. \qquad (1.36)$$

It is obvious that the last quantity in brackets is the compressor characteristic function that would apply in the absence of rotating stall; that is, the curve $\psi_c(\phi)$ shown on Fig. 1.1.

$$\psi_c(\phi) \equiv NF(\phi) - \frac{1}{2}\ \phi^2. \qquad (1.37)$$

It should be emphasized that while $\psi_c(\phi)$ is a given feature of the compressor, it is not the same as Ψ; the latter is the pressure rise actually produced, with rotating stall (if it occurs) in progress. While ψ_c is, in principle, given, it is not the characteristic usually measured in tests of compressors subject to rotating stall. One might rather say that Ψ is the usually-measured quantity; here, it is part of the answer.

The problem now is to find what values of parameters such as f, m, Ψ, or features of the function $\psi_c(\phi)$, permit nonzero solutions of the pair of equations (1.36) and (1.37).

Weak Disturbances

In this paper, we will restrict disturbances to be weak. Thus, we neglect the terms $(1/2)h^2$ and $(1/2)K_I h^2$ appearing in Eq. (1.36). Also, since ϕ will remain close to Φ during a weak disturbance, we keep only the first two terms of the Taylor series

$$\psi_c(\phi) = \psi_c(\Phi) + \psi_c'(\Phi)g + \frac{1}{2}\ \psi_c''(\Phi)g^2 + \ldots \qquad (1.38)$$

For convenience we define

$$\lambda \equiv \frac{2UN\tau}{D}\left(\frac{1}{2} - f\right) - \frac{U(\tau_{IV}+\tau_{OV})}{D} f \tag{1.39}$$

so that Eq. (1.36) becomes

$$\lambda g'(\theta) - mfh - \psi_c' g + \Psi - \psi_c(\Phi) = 0. \tag{1.40}$$

By definition, the average value of g over a cycle must vanish. Also, if the flow far upstream is purely axial, no average swirl can arise between there and the compressor entrance if the flow is irrotational. Therefore, the average value of h must also vanish. These conditions would apply even for strong waves, but in the present case, integrating Eq. (1.40) over a cycle shows that

$$\Psi - \psi_c(\Phi) = 0. \tag{1.41}$$

In other words, for weak waves, there is no vertical displacement of the operating point from the rotating-stall-free characteristic; it is as indicated for point A of Fig. 1.1.

Presumably, g and h have Fourier series with coefficients related by Eqs. (1.18a,c). Because Eq. (1.40) is linear, each coefficient is independently fixed. Using only the a_n terms, we find by substitution

$$(\lambda n - mf) a_n \cos n\theta - \psi'(\Phi)\, a_n \sin n\theta = 0. \tag{1.42}$$

The conditions for a weak periodic wave of arbitrary amplitude are therefore that $\lambda n = mf$, that $\psi_c'(\Phi) = 0$, and that $\Psi = \psi_c(\Phi)$. The first of these may be solved for propagation-speed coefficient f:

$$f = \frac{1/2}{1 + m\dfrac{D}{2UnN\tau} + \dfrac{\frac{1}{2}(\tau_{IV}+\tau_{OV})}{N\tau}}. \tag{1.43}$$

This is the chief result of our analysis, and will be discussed fully in the next section. The second requirement

$$\psi_c'(\Phi) = 0 \tag{1.44}$$

means that the local curve of ψ_c must be flat. This could be true in the deep-stall region (points like A or C in Fig. 1.1), and is true at the maximum of the characteristic (point M). In the latter case, Eq. (1.44) would be a condition for stall inception, agreeing with the classical stability requirement. On the descending branch of the speed line, Eq. (1.44) would not be satisfied; we interpret that to mean not that rotating stall cannot occur, but rather that it cannot be weak. In fact, ψ_c' can be interpreted as a negative damping factor; since Eqs. (1.18) indicate that $g = -h'$, Eq. (1.40) is that of a harmonic oscillator,

$$\lambda h'' - \psi_c' h' + mfh = 0$$

with homogeneous boundary conditions, a wave must decay if ψ_c' is negative, or be amplified if ψ_c' is positive. In neither case could a permanent oscillation exist.

Eqs. (1.41), (1.43), and (1.44) therefore give the conditions for a steady rotating stall of weak amplitude to exist, when reservoir pressures are both constant.

STALL PROPAGATION SPEED

We next discuss the implications of Eq. (1.41) and compare its predictions with experiment (2). Eq. (1.43) is essentially a balance of disturbance phase lags inside and outside the compressor.

The External Lag Parameter

The parameter m appears in Eq. (1.43). It was defined in Eq. (1.34) as a measure of the strength of the lagging pressure term fh arising in the exit duct. The same lag term arises from the entrance duct (the term fh in Eq. (1.21)) assuming ideal flow in a straight channel. We should admit the possibility that in the entrance flow, too, configuration or loss effects might affect lag. Thus, where the two lags are added to give mfh in Eq. (1.36), we should imagine m to be a net lag parameter depending on the combined contributions of both entrance and exit flows. We do nevertheless expect that it depends chiefly on the exit arrangement.

The Compressor Lag Parameter

The lag τ, defined in Eq. (1.3), depends on the aerodynamics of a blade passage, sketched in Fig. 1.2b. Whatever its physical nature, it should scale with axial passage length L and axial velocity V. We are then led to define a dimensionless lag

$$\tau^* \equiv \frac{\Phi U \tau}{L} \tag{1.45}$$

in terms of which Eq. (1.43) becomes

$$f = \frac{1/2}{1 + \frac{m\Phi}{n}\frac{D}{2NL}\frac{1}{\tau^*} + \frac{1}{N}\frac{\tau_v^*}{\tau^*}} . \tag{1.46}$$

The lags for guide vanes are assumed equal.

It is perhaps of interest to note the value of τ^* that would represent "apparent mass" or inertia only. Referring to Fig. 1.2b, we see that a mass $\rho L\sigma/\cos\gamma$ of fluid is accelerating in a blade passage at a rate $U\dot{\phi}/\cos\gamma$ requiring the force provided by an additional pressure rise $(\Delta p)_A$:

$$\frac{(\Delta p)_A}{\frac{1}{2}\rho U^2} = -\frac{2}{\cos^2\gamma}\frac{L}{U}\dot{\phi} . \tag{1.47}$$

Comparing Eq. (1.3) we see that, due to inertia in blade passages only, $\tau^* = 2\Phi/\cos^2\gamma$. The stagger angle γ is roughly $\tan^{-1}(1/2\ \Phi_d)$ where Φ_d is design flow coefficient. We write

$$\tau^* = \frac{2\Phi}{\cos^2\gamma}\ k \tag{1.48}$$

where a factor k has been included because, often, the interrow gap is quite large. If the gap were a multiple k-1 of L, then τ^* would be proportional to k.

Other effects having to do with separation or secondary flows will also influence τ^*. If these could be represented by suitable choice of k, it would be appropriate to write Eq. (1.46) in the following form:

$$f = \frac{1/2}{1 + \frac{m}{k}(\cos^2\gamma)\,\frac{1}{2n}\,\frac{D}{2NL} + \frac{\tau_v^*}{\tau^*}\,\frac{1}{N}} \,. \qquad (1.49)$$

We will use k as a general "uncertainty factor" comparing actual τ to blade-passage inertia lag. It is interesting that the external and internal lag parameters enter Eq. (1.49) only in their ratio, m/k.

Qualitative Results for Propagation Speed

Eq. (1.46) shows certain general trends:

1. Propagation speed is less than 50 percent of U, unless τ is negative. Actually, negative lag has been argued to occur at stall of isolated airfoils (11), and $f > 1/2$ is generally associated with single-stage experiments (2,5). Perhaps these results are consistent.

2. Increasing number of stages (N) increases f toward 1/2. This result has been found by Cumpsty and Greitzer (9). It is important that N multplies τ^* in Eq. (1.46). If τ is very small, being proportional to blade chord, it might at first be thought to make a negligible contribution to pressure rise (Eq. (1.3)), and therefore not be proper to include in a disturbance analysis. This argument might be valid for single-row problems. However, a small lag per row will accumulate over many rows in a multistage compressor to make a large overall lag; it is the latter which governs rotating stall. The same idea is expressed by noting the group D/2NL in Eq. (1.49); it describes the shape factor of the whole compressor when viewed from the side. Typically, it would be of order 1, while for a single row, D/L would be much larger--typically about 15.

3. Multicell stalls have higher propagation speeds. The mode number n represents number of stall cells.

4. Increased lag (larger k) tends to increase propagation speed.

5. Especially if design flow coefficient Φ_d is small, smaller Φ_d (or larger stagger angle) will increase f.

6. If the net external phase-shift parameter m is made smaller, f is increased. For a typical engine, m is probably near 2. If the diffuser is a sudden area change at the rear face of the compressor, m = 1. If circumferential velocity were suppressed in the inlet flow, m might also decrease by 1. A value of m = 0 may be theoretically possible, if circumferential velocity is suppressed in both entrance and exit flows.

7. Guide vanes have little effect on f in multistage compressors.

Comparison with Day and Cumpsty's Data

The foregoing results may be compared with the propagation speed data of Day and Cumpsty (2). Table 1.1, in the first 5 columns, collects some of their results for various designs, number of stages, and number of stall cells. Of single-cell cases (n = 1), only the full-span results are included, because the present paper assumes full-span stall, in effect. Multiple-cell cases are included, but it should be noted that all of them are part-span. Guide vanes have a smaller average incidence than core blades, by about a factor of 2. Therefore relative velocities are lower. As a rough estimate, we will assume τ_v to be the average of Eq. (1.48) and $2\Phi k$. In that case,

$$\frac{\tau_v^*}{\tau^*} = \frac{1}{2}\,(1 + \cos^2\gamma) \quad .$$

For the experiments (2) the blade chord is 17.8 mm, and the mean diameter is about 320 mm. The spacing between rows is about one chord width. In that case, if inertia were the only source of lag, we would expect k = 2. There appears to be a fairly long straight section before the diffuser, and so one would expect m = 2. Eq. (1.49) shows that k and m enter in the ratio k/m. The last two columns of numbers are the theoretical predictions of Eq. (1.49) for two values of k/m, the first being for the expected k/m = 1 (k = 2, m = 2), and the second for k/m = 2. The latter would apply if k were 4 instead of 2 owing to separation hysteresis, or perhaps if the exit acted like an orifice so that m = 1 instead of 2. The former would be a more likely combination (m = 2, k = 4).

Comparing the theoretical and experimental columns, it is clear that Eq. (1.49) gives all the proper trends of f with γ, N, and n. We should keep in mind that the theory does not contemplate the part-span stall patterns found experimentally for multiple zones, so agreement for n different from 1 is perhaps fortuitous. The theory probably does not apply well to single-stage situations. Therefore, the most appropriate comparisons are for n = 1, N = 2,3,4. These cases are enclosed in boxes in the Table, for emphasis.

Table 1.1 clearly indicates that k/m = 2 is the best choice for agreement, and the agreement could hardly be closer, for intermediate and high-Φ_d builds. For low Φ_d, full agreement would require a somewhat higher value of k/m, about 3 instead of 2. Perhaps the higher stagger angle causes more hysteresis due to separation.

In the low-Φ_d experiments, a reduced spacing gave a substantailly lower speed. In that case, we would expect to reduce the factor k to account for the smaller mass of fluid undergoing oscillation. Because

spacing was originally one chord length, it seems reasonable to reduce k by a factor of 2. Indeed, Table 1.1 shows that k/m = 1 gives a prediction having the same relation to experiment for reduced spacing as k/m = 2 had for the wider spacing. Also, it was mentioned that k/m = 3 gives exact agreement with experiment for the wider spacing; k/m = 1.5 gives exact agreement for reduced spacing. Thus, we may add spacing to the list of compressor parameters whose influence on propagation speed is well predicted by Eq. (1.49).

Finally, we should note that Cumpsty and Day (9) have derived an equation for propagation speed based on a consideration of pressure jumps across the boundaries of deep-stall zones, together with certain observations of compressor test results. Their equation also predicts the correct trend with number of stages.

CONCLUDING REMARKS

The present analysis shows that rotating stall can be considered an eigenfunction of a compressor-inlet-diffuser system if a single lag process occurs in the generation of force by a blade passage, and, at least for weak amplitude, if there is a flat total-to-static pressure rise characteristic in the neighborhood of the average flow coefficient set by the throttle.

The predicted propagation speed depends on various features of the compressor, and follows very closely the trends of experimental observations as those features are changed. The lag processes originating in the compressor (k) and those originating outside the compressor in the entrance duct and the diffuser (m) require more study from a fundamental point of view.

The present analysis, being based on small perturbations, has limited value. First, actual perturbations in deep stall are not small, nor are amplitudes arbitrary. Therefore, there is little guidance from the present analysis as to how compressor parameter changes might help to control or eliminate the phenomenon. However, the results of the present analysis perhaps do give encouragement for the study of finite amplitude oscillations using similar physical assumptions.

Parts II and III of this study report such extensions. In Part II, we keep the restriction to a flat characteristic, but allow the amplitude to be finite. Results will include a measure of how the mean performance is affected by the existence of rotating stall, as well as certain interesting velocity and pressure profiles. In Part III, we attempt to relate rotating stall to the complete characteristic curve. Results include an indication of when the "blockage" model (3) applies, and also predict that rotating stall becomes impossible beyond some value of flow coefficient, probably indicating the onset of stall recovery.

TABLE 1.1. PROPAGATION SPEED COEFFICIENT

Φ_d	γ (degr)	N	n	f (percent)		
				Ref 2	Eq. (1.49)	
					k/m = 1	k/m = 2
0.35	50	1	1	19	11	16
			6	31	23	26
			12	66	26	27
0.35	50	3	1	[32]	23	[29]
			4	40	34	37
			12	60	38	39
0.35	50 (reduced spacing)	3	1	[27]	[23]	29
			5	54	35	38
0.55	35	1	1	15	9	14
		2	1	[22]	15	[21]
		3	1	[26]	20	[26]
		4	1	[31]	23	[30]
1.00	20	1	1	11	8	12
		2	1	[20]	14	[20]
		3	1	[24]	18	[25]
		4	1	[28]	22	[28]

Chord = 17.8 mm
Mean diamater: 320 mm

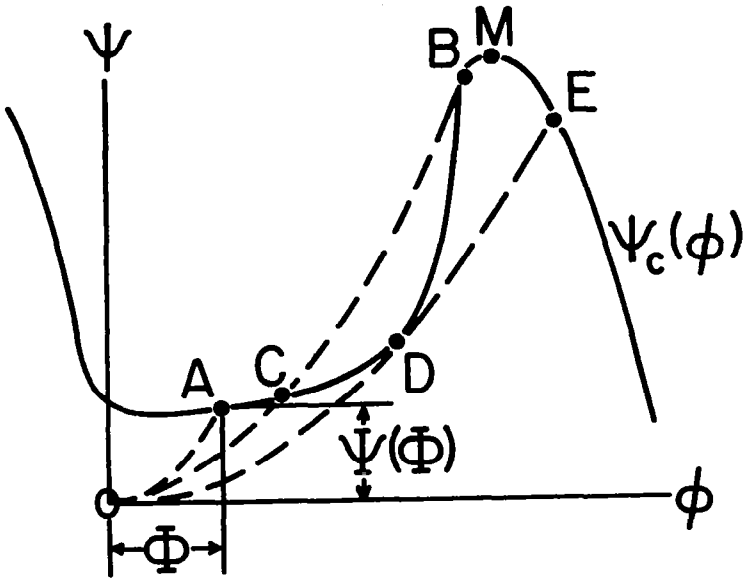

Fig. 1.1. Constant-speed compressor characteristic $\psi_c(\phi)$, and operating points $\Psi(\Phi)$; upstream total to downstream static pressure rise versus axial flow coefficient.

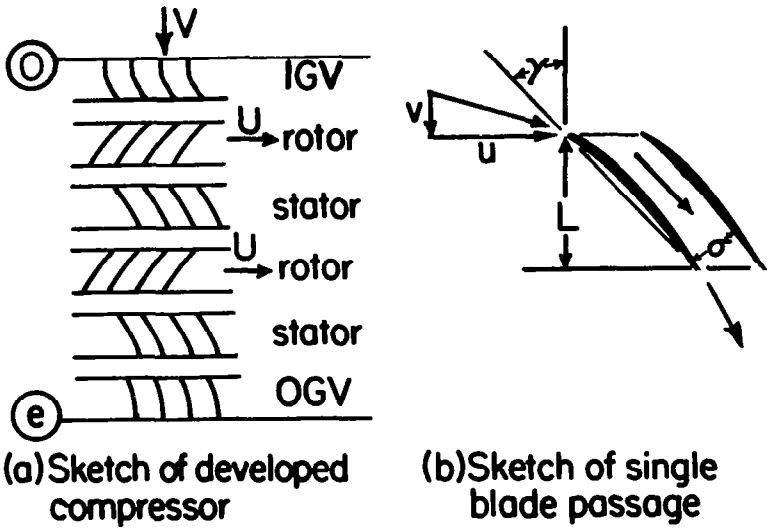

Fig. 1.2. Sketch of compressor configuration. Number of stages is arbitrary; two are shown. Radial effects are neglected. Entrance and exit planes are denoted by ⓞ and ⓔ. Blading is symmetrical.

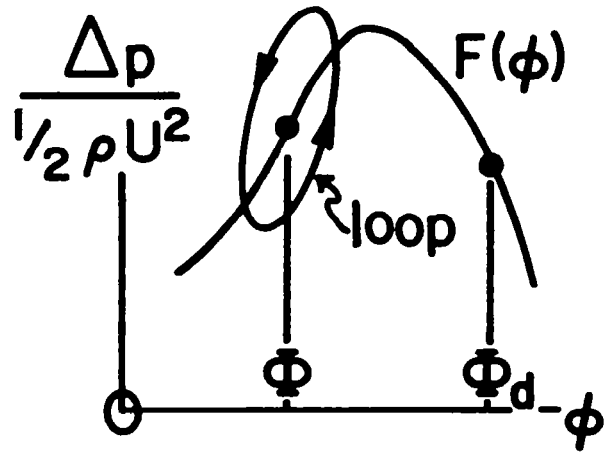

Fig. 1.3. Assumed form of blade-passage pressure-rise function.

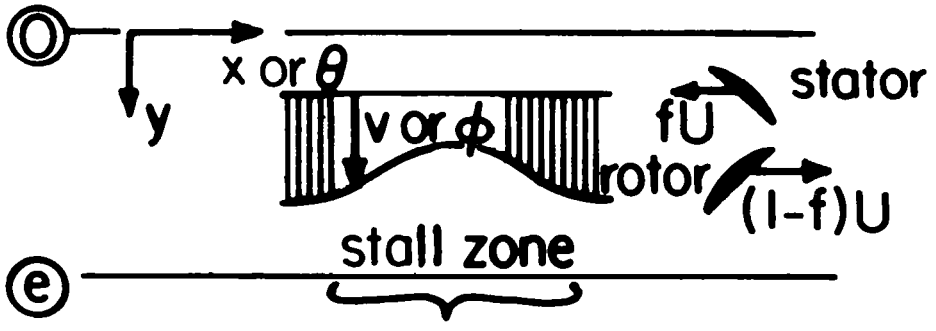

Fig. 1.4. Sketch showing axial stall zone in compressor, in coordinates fixed in the stall zone which, in laboratory coordinates, is moving to the right at speed fU.

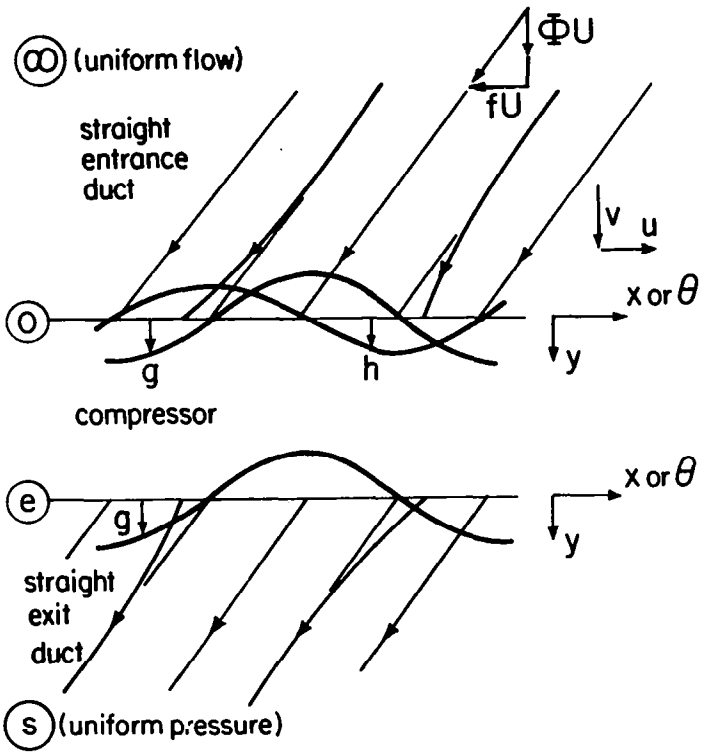

Fig. 1.5. Sketches of flows in straight entrance and exit ducts, coordinates fixed in disturbance. At the compressor exit, $u = -fU$.

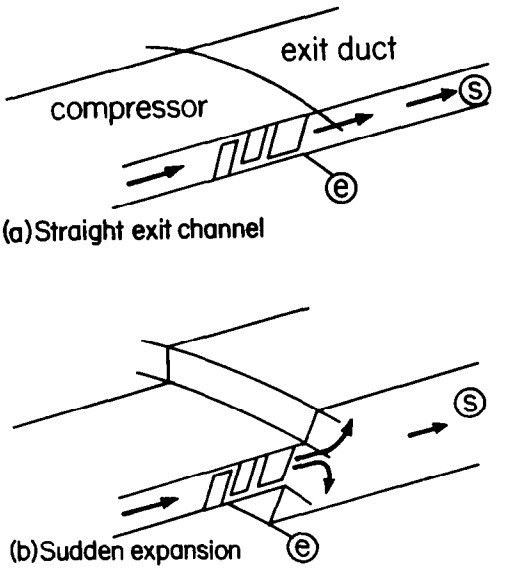

Fig. 1.6. Sketches of extreme exit-duct configurations.

PART II - FINITE DISTURBANCES

SUMMARY

A small-disturbance theory of rotating stall in axial compressors is extended to finite amplitude, assuming the compressor characteristic is a parabola over the range of the disturbance. An exact solution is found which requires the operating point to be at the minimum or maximum of the parabola.

If the characteristic is flat in a deep-stall regime, the previous harmonic solution applies with neither reverse flow or "unstalling". If the characteristic is concave upward in deep stall, the disturbance has a skewed shape, steeper at the stall-zone trailing edge as experiment shows. Propagation speed is only slightly affected by this nonlinearity.

Near stall inception, negative curvature in combination with multiple stall zones can limit the nonlinear oscillation, in the manner of "progressive" stall. If, as seems likely, lag at stall inception is negative (opposite to inertia), propagation speed exceeds 1/2 wheel speed, as experiments suggest.

INTRODUCTION

In Part I ("Small Disturbances"), it was shown how a combination of three lags, pertaining to entrance-flow passage, compressor blade passage, and exit-flow passage permit the occurrence of a flow distortion which is steady in a moving frame of reference. In principle, the entrance and exit lags are easily calculated, while the blade-passage lag is difficult to define and infer from tests. Comparison with measurements of rotating-stall propagation speed made by Day and Cumpsty (2) support the idea that the blade-passage effect is largely inertial, in deep stall.

The lag per row was represented as a factor k of the purely inertial value for a blade passage. If the inter-row gap is equal to the blade depth then k would be about 2, still considering only inertia but including the mass of fluid occupying the inter-row space. The combined lag effect of entrance and exit flows was represented by the factor m; if long straight passages describe both entrance and exit configurations, then m = 2.

For small perturbations, k and m enter as a ratio in the formula for propagation speed. If the ratio is taken as 2 (about twice what we would expect on purely inertial grounds), agreement with experiment is very complete, suggesting that a single compressor lag parameter, if suitably chosen, could lead to a quite complete description of rotating stall.

Small perturbations restrict wave forms to be harmonic, which is quite unlike the wave forms actually observed (2). Furthermore, the amplitude is unspecified in a linear analysis. Thus, although a good prediction of propagation speed is encouraging, the important questions about rotating stall have to do with disturbances of finite amplitude. Specifically,

1. What is the effect on average pressure-rise performance caused by rotating stall?

2. Are there circumstances which limit the amplitude of oscillation? If so, "progressive stall" may be indicated.

3. Are there ranges of flow coefficient for which rotating stall is forbidden? If so, "stall recovery" may be indicated.

In considering these questions, we should, if possible, allow the assumed compressor characteristic to depart from a constant value during the oscillation of flow coefficient. In this part, we investigate the finite-strength disturbances permitted when the characteristic is either flat or has constant curvature.

SOLUTIONS OF THE PRESSURE EQUATION

The Disturbance Equations

We recall the basic pressure-match equation, Eq. (1.36) of Part I, and incorporate Eqs. (1.37) and (1.39):

$$\lambda g'(\theta) - mfh + \frac{1}{2}(1-K_I)h^2 + \Psi - \psi_c(\phi) = 0 \qquad (2.1)$$

where g and h are the axial and circumferential velocity disturbances, related by the Fourier series (Eq. (1.18)), or the equivalent statement

$$h + ig = \text{analytic function of } (e^{i\theta}). \qquad (2.2)$$

We will assume that the rotating-stall-free characteristic function remains well represented, over the range of the oscillation, by the first three terms of a Taylor series (Eq. (1.38)) about the mean flow Φ:

$$\psi_c(\phi) = \psi_c(\Phi) + \psi_c'(\Phi)g + \frac{1}{2}\psi_c''(\Phi)g^2 + \ldots \qquad (2.3)$$

We will find that no solutions are possible unless $\psi_c'(\Phi) = 0$, even for finite disturbances. Such a term would represent a damping effect, even for finite disturbances, and must be discarded if only the three terms of Eq. (2.3) are considered. The reasons why this is true will be made clear later, especially in Part III.

Eq. (2.1) now becomes

$$\lambda g'(\theta) - mfh + \frac{1}{2}(1-K_I)h^2 - \frac{1}{2}\psi_c''(\Phi)g^2 + \delta = 0 \qquad (2.4)$$

where δ is the performance increase (perhaps negative) due to rotating stall:

$$\delta \equiv \Psi - \psi_c(\Phi). \qquad (2.5)$$

A typical function $\psi_c(\Phi)$ and positive δ are sketched in Fig. 2.1.

The second term of Eq. (2.4) embodies the factor m, introduced in Part I to account for lags external to the compressor. This factor was found to be 2 for small disturbances of a straight-channel exit. In the present part, we are concerned with finite disturbances, and a more complete accounting for downstream pressure recovery is no doubt needed. The necessary analysis would be very arduous, and not justified for a particular highly-idealized exit channel. For a sudden exit expansion, we argued that m = 1, and this result is independent of amplitude. Therefore, the term mfh will be retained because it is proper when m = 1, and may be empirically justified for other values of m. Further research on this point is required.

The disturbances g and h governed by Eq. (2.4) are periodic (but not necessarily harmonic) and have vanishing averages over a cycle; in the case of g because it is defined as a departure from average axial velocity, and in the case of h, because net circulation in the entrance flow is assumed to remain zero. Therefore, integrating Eq. (2.4) over a cycle shows that, when nonlinear terms involving h^2 and g^2 are included, the constant δ cannot be zero, as it was in the linear analysis of Part I.

A General Solution

In Part I, Eqs. (2.2) and (2.4) had a simple harmonic solution because the last three terms of Eq. (2.4) were absent. Here, those terms are kept, and appropriate nonlinear periodic solutions are sought.

It happens that a general solution, believed to be unique, can be written down at once:

$$h + ig = A \frac{e^{in\theta}}{1 + \eta e^{in\theta}} \tag{2.6a}$$

or

$$h = \frac{A(\cos n\theta + \eta)}{1 + \eta^2 + 2\eta \cos n\theta} \; ; \quad g = \frac{A \sin n\theta}{1 + \eta^2 + 2\eta \cos n\theta} \tag{2.6b}$$

where A and η are constants to be determined by satisfying Eq. (2.4). In order that h and g have Fourier series in θ of the form of Eq. (1.18), it is necessary that $|\eta| < 1$. Eq. (2.6a) is clearly a special case of Eq. (2.2) and the previous linear solution is recovered by setting $\eta = 0$.

The forms of these velocity traces are shown for various values of η between 0 and 1, on Fig. 2.2. The axial-flow disturbance g is antisymmetric and is traveling to the right. Its negative portion represents a "stall zone"; if A is positive, its "trailing edge" is steeper.

In presenting the results for A and η obtained by substitution into Eq. (2.4), we note that f is not known, and recall that

$$\lambda = \frac{2UN\tau}{D} \left(\frac{1}{2} - f\right) - \frac{2U\tau_v}{D} f \tag{2.7}$$

if the lags for IGV and OGV are equal. Thus, a free constant will remain after η, A, and δ are given in terms of f. Results are

$$\frac{\lambda n}{mf} = \frac{(1-\eta^2)\psi_c'' + (1-5\eta^2)(1-K_I)}{(1+\eta^2)\psi_c'' + (1-3\eta^2)(1-K_I)} \tag{2.8}$$

$$A = \frac{4mf}{\psi_c''} \eta \frac{(1-\eta^2)\psi_c'' + (1-3\eta^2)(1-K_I)}{(1+\eta^2)\psi_c'' + (1-3\eta^2)(1-K_I)} \tag{2.9}$$

$$\delta = \frac{Amf}{8\eta^2}\,[4\eta - Amf(\psi_c'' + 1 - K_I)]. \tag{2.10}$$

The next step will be to describe rotating-stall features implied by Eqs. (2.8-10). First, we should specify the parameters $\psi_c''(\Phi)$ and K_I.

In these equations, K_I is the coefficient of pressure recovery in the entrance of the IGV passage, owing to the fact that a transverse velocity disturbance makes an incoming stream tube somewhat narrower than the IGV entrance. Fig. 2.3 sketches the process. The conservative estimate of this effect is gotten by assuming the area increase is sudden. The usual pressure-rise formula in such a case is

$$\frac{\Delta p}{\rho(V^2+u^2)} = \frac{A_1}{A_2}\left(1 - \frac{A_1}{A_2}\right)$$

but the geometry of Fig. 2.3 shows that $A_1/A_2 = V/\sqrt{V^2+u^2}$. Since $V = U\phi$ and $u = Uh$ in stator coordinates, we may conclude that

$$\frac{\Delta p}{\rho U^2} = \phi^2\left[\sqrt{1+(h/\phi)^2} - 1\right] = \frac{1}{2}\,h^2 K_I, \tag{2.11}$$

the last member of the equation being the definition of K_I. The quantity $1-K_I$ which appears in Eqs. (2.8-10) is the head loss coefficient due to oblique entrance to the IGV. Clearly, it is a function of h itself, and therefore cannot properly be used in Eq. (2.4) as a constant. Fortunately, the magnitude of $1-K_I$ is very small, not exceeding 0.1, by Eq. (2.11), unless h/ϕ exceeds 0.7. Therefore, one is justified in neglecting the head-loss effect represented by $1-K_I$, and Eqs. (2.8-10) become:

$$\frac{\lambda n}{mf} = \frac{1-\eta^2}{1+\eta^2} \tag{2.12}$$

$$A = \frac{4mf}{\psi_c''}\,\frac{\eta(1-\eta^2)}{1+\eta^2} \tag{2.13}$$

$$\delta = \frac{4(mf)^2}{\psi_c''}\,\frac{\eta^2(1-\eta^2)}{(1+\eta^2)^2}\,. \tag{2.14}$$

We bear in mind that λ is a given function of f (Eq. (2.7)) and therefore Eq. (2.12) is an equation connecting f and η. In fact, Eq. (2.12) may be replaced by

$$f = \frac{1/2}{1 + \frac{\tau_v/\tau}{N} + \frac{am}{n}\frac{1-\eta^2}{1+\eta^2}} \tag{2.15}$$

where the symbol a is introduced to define the group

$$a \equiv \frac{D}{2UN\tau} = \frac{D}{NL}\frac{\Phi}{2\tau^*} \tag{2.16}$$

and the last expression results from Eq. (1.45). In discussing compressors of many stages, one might well neglect the second term of the denominator of Eq. (2.15), finding

$$f = \frac{1/2}{1 + \frac{am}{n}\frac{1-\eta^2}{1+\eta^2}} . \tag{2.17}$$

Pressure Disturbance

We should record for subsequent use an expression for pressure-rise fluctuation, because that is a quantity more easily measured than the velocity components represented by g and h. Eqs. (1.8) and (1.9) and the present Eqs. (2.4) and (2.5), with $K_I = 1$, yield the static pressure rise across the compressor:

$$C_p \equiv \frac{p_e - p_o}{\rho U^2} - [\tfrac{1}{2}\Phi^2 + \Psi(\Phi)] = -mfh + \Phi g + \tfrac{1}{2}g^2 + \tfrac{1}{2}h^2. \tag{2.18}$$

Included in brackets on the left of this equation are certain quantities which will be constant during any rotating-stall process. Quantities which will fluctuate are on the right side, and they are the ones of most interest.

Amplitude of Solution

We have noted that Eq. (2.6b) describes an oscillation of axial flow (g) that is symmetrical: its amplitude can be found using Eqs. (2.13) and (2.17) to be

$$g_m = \frac{2m}{\psi_c''} \frac{\eta}{(1 + \frac{am}{n}) + \eta^2(1 - \frac{am}{n})} \tag{2.19}$$

with η being an amplitude parameter as yet undetermined.

As a function of η, the disturbance amplitude g_m might be limited in some circumstances. According to Eq. (2.19), the maximum value that g_m can assume is

$$g_{mm} = \frac{m}{\psi_c''} \frac{1}{\sqrt{1-(am/n)^2}} \tag{2.20}$$

when

$$\eta_{mm} = \sqrt{\frac{1-(am/n)}{1+(am/n)}} \ . \tag{2.21}$$

In such a case, Eqs. (2.17) and (2.14) give

$$f_{mm} = \frac{1/2}{1 - (am/n)^2} \ ; \ \delta_{mm} = - \frac{m^2}{\psi_c''} \frac{am/n}{[1 - (am/n)^2]} \ . \tag{2.22}$$

Because η is restricted to be less than 1, Eq. (2.21) shows that this particular limiting solution is possible only if a is negative, and that requires τ to be negative; in effect, the hysteresis loop of Fig. 1.3 would be clockwise in such a case.

If, on the other hand, a is positive, Eq. (2.19) shows that maximum would occur when $\eta = 1$, taking the value $g_{mm} = m/\psi_c''$.

Next, we should apply these results for interesting choices of ψ_c'', indicated on Fig. 2.1. There are two types of points where the characteristic (in absence of rotating stall) is horizontal ($\psi_c'(\Phi) = 0$) but yet has nonzero curvature. They are indicated on Fig. 2.1 as points C and M. At point C, the curvature $\psi_c''(\Phi)$ is positive, while at M it is negative.

DEEP STALL

Flat Characteristic

At a point such as C of Fig. 2.1, we first consider the possibility that $\psi_c'' = 0$ everywhere in the range of oscillation. In that case, Eq. (2.19) shows that η must be zero if g_m is to be finite, and Eqs. (2.17) and (2.14) give

$$f = \frac{1/2}{1 + (am/n)} ; \quad \delta = 0. \tag{2.23}$$

This is simply the harmonic solution discussed in Part I, with, according to Eq. (2.6b),

$$h = g_m \cos n\theta; \quad g = g_m \sin n\theta.$$

We conclude that in a region where the characteristic is flat, the solution is the linear one with arbitrary amplitude, even though a nonlinear solution is allowed. This result perhaps explains the surprising outcome of Part I, that a small-perturbation theory yields a good representation of stall propagation speed, even though the actual stall amplitude is large. For realistic comparison with experiment, the lag τ, and hence a, is positive, corresponding to values of $f < 1/2$.

The amplitude cannot actually be unlimited, of course. We suppose that this linear solution will be appropriate for rather small mean flow coefficients, so that the oscillation does not intrude into the rising part of the characteristic, with "unstalling" becoming a feature of the oscillation. In the same way, we would forbid the flow to reverse, imagining an abrupt rise of the characteristic below $\phi = 0$. If this is true, the oscillation should have an amplitude limited by Φ itself. That is,

$$h = \Phi \cos n\theta; \quad g = \Phi \sin n\theta. \tag{2.24}$$

Although the velocity components are harmonic, the pressure fluctuation is not, according to Eq. (2.18): If $n = 1$,

$$C_p = \frac{1}{4}\Phi^2 - mf\,\Phi \cos\theta + \Phi^2 \sin\theta. \tag{2.25}$$

If, for example, $\Phi = 0.4$, $a = 0.4$, and $m = 2$, the velocity and pressure-rise fluctuations would be shown in Fig. 2.4. The pressure trace is also harmonic. The propagation is toward the right of the figure, at a speed (f) of 0.278. In this case, of course, $\delta = 0$, because $\eta = 0$. The operating point lies at point C, on the characteristic, as indicated in the sketch.

Concave Characteristic

Next we consider the possibility that $\psi_c''(\Phi)$ is slightly positive, or concave, as at point C of Fig. 2.1. Again, we expect that a is positive (on the ground that deep stall seems always to have $f < 1/2$). In that case, the greatest possible value of η would be 1, but then only if ψ_c'' is larger than m/g_m according to Eq. (2.19). For realistic diagram shapes, ψ_c'' must be much less than m/Φ, and we therefore conclude that η is quite small in these cases.

From Eq. (2.19), setting $g_m = \Phi$ and making η small gives

$$\eta = \frac{\psi_c''}{2m}\left(1 + \frac{am}{n}\right). \tag{2.26}$$

Substitution of Eq. (2.26) into previous equations will give corrections of order ψ_c'' to the flat-characteristic solutions. While the predicted traces of g and h, as well as δ, will change to first order in ψ_c'', the value of f will be affected only to second order.

If $\psi_c'' > 0$, then A is positive and the velocity traces are as in Fig. 2.2, with an axial flow disturbance (g) which is steepest at the stall-zone "trailing edge", as experiments have shown (2). By way of example, we modify the example displayed in Fig. 2.4, by making $\psi_c''(\Phi) = 1.65$; the changed characteristic is sketched in Fig. 2.5. Eq. (2.18) gives the corresponding pressure trace C_p. Pressure rise as well as axial velocity demonstrate the steep "trailing edge" found experimentally.

INCIPIENT STALL

Convex Characteristic

At a point such as M, the value of ψ_c'' is negative. At a given speed, as flow coefficient Φ is reduced, rotating stall can first appear at point M. The characteristic of Fig. 2.1 is drawn to show some degree of overturn to the left of M, terminated in an abrupt drop at point B. At that point, we imagine a certain positive slope S to occur. The final slope S depends on the compressor; lightly-loaded

compressors tend to permit a larger S before a steep break occurs. If a parabola is used to represent the curve in the stall-inception zone, centered on point M, one could relate S to ψ_c'' and the distance $\Delta\Phi$ between points B and M on the diagram:

$$\Delta\Phi = S/\psi_c''. \tag{2.27}$$

As we have seen, a stall oscillation about point M would have a maximum permissible amplitude g_{mm} depending on the sign of τ (or a):

$$\left.\begin{aligned} g_{mm} &= \frac{m/\psi_c''}{\sqrt{1 - (am/n)^2}}, \quad a < 0 \\ &= m/\psi_c'', \quad a > 0 \end{aligned}\right\} \tag{2.28}$$

If this maximum amplitude exceeds the $\Delta\Phi$ between points B and M, then the oscillation could easily extend into the deep stall zone, and a different type of larger-amplitude oscillation would result, of the sort to be discussed in Part III of this report. On the other hand, if $g_{mm} < \Delta\Phi$, the oscillation could be limited to the vicinity of point M, governed purely by the local convex parabolic segment. This latter situation would presumably relate to "progressive" stall.

Because $\psi_c''(\Phi) < 0$, Eq. (2.13) shows that $A < 0$. Thus, the trace of g in Fig. 2.2 is reversed in sign, and now it is the cell "leading edge" that is the steeper. The proper value of η can be found from Eq. (2.19), if g_m is fixed.

Progressive Stall

Pursuing this idea further, we can relate g_{mm} and $\Delta\Phi$ from Eqs. (2.27), (2.28) to arrive at the criteria for limited, or progressive-type stall:

$$S > \frac{m}{\sqrt{1 - (am/n)^2}}, \quad a < 0 \tag{2.29}$$

$$S > m, \quad a > 0. \tag{2.30}$$

These equations indicate that progressive stall is favored if

1. S is large. Experience confirms that a delayed "break," and hence large S favors progressive stall.

2. m is small. That is, an abrupt expansion at exit as opposed to a long, straight discharge would favor progressive stall. It is not known whether experience confirms this prediction.

3. n is large, if $a < 0$ (clockwise hysteresis). Large n denotes many stall cells, and experience is quite definite that progressive stall is associated with multiple stall cells (2). We find that n is relevant only if $a < 0$ and, therefore, $f > 1/2$ (Eq. (2.22)). It is also usually found that progressive stall has this feature as well (see Ref. 2 or Table 1.1), and we conclude that clockwise hysteresis ($a < 0$, $\tau < 0$) is quite typical in these "soft-stall" cases. Theoretically, it has been argued (11) that lift hysteresis of a single airfoil is of this sense if its stall process is a progressive advance of trailing-edge separation as opposed to the more abrupt leading-edge stall. In the former case, lift curves are rounded, while in the latter case, an abrupt break occurs. Thus, there is some basis for expecting $\tau < 0$ for progressive compressor stall.

4. a is small, if $a < 0$. Actually, am and n should be considered together; Eq. (2.17) provides

$$\frac{am}{n} = \frac{Dm}{2UNn\tau} \quad . \tag{2.31}$$

This grouping suggests that large τ favors progressive stall, as does a large product Nn. Perhaps it may be inferred that large n is especially required for single-stage ($N = 1$) progressive stall, whereas multistage machines can have progressive stall which does not split up into multiple cells because Nn is large even if $n = 1$. Experimental results tend to support this idea.

Fig. 2.6 shows velocity and pressure-rise fluctuations calculated for a limited oscillation of the sort just discussed; with a negative and ψ_c'' quite large and negative. n was taken to be 4, and the stall point M was considered to occur at $\Phi = 0.8$. The amplitude is only 0.053, but η is quite large because ψ_c'' is large, and the traces are quite far from harmonic shape. Propagation speed is greater than 1/2, and axial velocity changes most rapidly at the cell leading edge, in contrast to the case when $\psi_c'' > 0$. This result is in contrast to the known tendency of deep-stall wave forms to be steeper at the cell trailing edge (3). Probably, the differing curvatures of ψ_c are important in this regard. Perhaps it would be useful to investigate this aspect of progressive stall experimentally.

Limitations of the Analysis

Multi-cell progressive stall is usually also part-span stall (2). The present analysis assumes two-dimensional flow; in effect, full-span disturbances are assumed. The importance of this inconsistency with observations is difficult to assess.

The foregoing analysis does not show that rotating-stall oscillations must extend to the allowed amplitude limits, or that the oscillation will choose, so to speak, to adopt a zone number appropriate to progressive stall. Neither is it shown that the oscillation will become of the large-amplitude type just because it is not limited to remain above point B. These questions are ones for future research, probably to be answered by studying limit cycles emerging from Eq. (2.4). The present analysis is intended to suggest features to look for, in those more complete and inevitably more complex and confusing solutions.

Finally, we should recall the criterion $\psi_c'(\Phi) = 0$ mentioned following Eq. (2.3). Of course, a throttle setting need not correspond to $\Phi'(\Phi) = 0$. However, a purely period wave cannot occur, governed by a purely parabolic characteristic unless that is true, even if the motion is nonlinear. The reason for this result, which will be made clear in Part III, is essentially that mentioned in Part I; namely, that $\psi_c'(\Phi)$ would be an amplification coefficient in Eq. (2.3). If $\psi_c'(\Phi) > 0$, then any oscillation would grow until it encountered new features of the function $\psi_c(\Phi)$, beyond the range of the assumed parabola, such as a resistance to reversed flow, and this encounter would lead finally to a limit cycle. If $\psi_c'(\Phi) < 0$, then the oscillation would presumably disappear by damping.

Thus, if Φ is intermediate between points B and M, rather than at M, an oscillation would presumably amplify to include some involvement with the steep drop at B. This case is beyond the scope of this paper.

CONCLUDING REMARKS

Finite-amplitude rotating stall has been analyzed for cases in which it may be assumed that the constant-speed characteristic is parabolic in flow coefficient with rotating stall absent. It was found that a periodic solution (neither damped nor amplified) requires a horizontal slope of that characteristic at the given average flow. Presumably, if the slope were negative, the oscillation would be damped, but if it were positive, the oscillation would grow until new features of the characteristic curve (reverse flow or stall recovery) become influential.

In "deep stall," if the characteristic is flat, the solution differs only slightly from the linear one, perhaps explaining why

propagation speeds from Part I agree so well with experiment. In this case (Figs. 2.4 and 2.5), the oscillation would presumably be limited by reverse-flow resistance, provided flow coefficient is quite low (less than half the coefficient at stall). At larger flow coefficients, even if the characteristic is locally flat, interaction with the unstalled part of the characteristic will occur, and the resulting motion will become non-harmonic on that account. This is the subject of Part III of this report.

The characteristic function $\psi_c(\phi)$ we have used is artificial in the sense that it is defined in the absence of rotating stall, and therefore is not normally measured in compressor tests. However, it is perfectly well defined physically, and could be measured in experiments designed to suppress rotating stall. It is defined for the compressor alone, and therefore one is free to manipulate exit and entrance conditions in order to prevent rotating stall, and also to eliminate any irrelevant hysteresis effects of a control throttle.

In incipient stall conditions, the stall oscillation may be limited in amplitude by a strong reverse curvature of the characteristic, permitting a progressive type of stall. If the characteristic "turns over," so that the break of the speed line is delayed substantially below maximum pressure rise, then this limited solution is favored. If the force lag is negative (opposite in sense to the effect of inertia) then two notable results appear: The propagation speed exceeds 1/2 U, and the limited-amplitude solution is favored for multiple cells. Because experiments usually show these same features, the inference seems warranted that lag (τ) is indeed negative in the incipient or progressive stall region.

In the deep-stall region, nonlinearity associated with concave curvature of the characteristic provides a steepening of the stall-zone trailing edge, as experiments show, provided lag (τ) is positive. Probably, then, lag should be taken positive in deep stall, and negative in incipient stall. Experiments are needed to establish these blade-passage lags.

Theory and experiment are both needed to describe the entrance and exit flows, especially for the relation between axial and transverse velocity disturbances. The present theory shows that rotating stall is sensitive to these conditions (lumped, in the present theory, in the parameter m), and practical control means could well evolve from such a study.

A new type of experiment is needed to find the compressor characteristic in the absence of rotating stall, and free of irrelevant throttle hysteresis. Experiments have suggested that exhaust to

low pressure through a high-resistance screen may suppress rotating stall even at fully-stalled flow rates, and also that unwanted throttle effects can be eliminated by lowering pressure behind the throttle (see Ref. 3, Fig. 19). Therefore, it seems feasible in principle to measure $\psi_c(\phi)$.

The present theory shows that the characteristics with and without rotating stall are different (δ represents that difference) and thus that rotating stall affects average compressor performance. Ultimately one can envisage a theory in which surge and rotating stall are integrated, rather than being considered separate and independent phenomena. One would then be able to deal with engine dynamics on a fundamental basis.

A nonlinear, unsteady model of rotating stall has in fact been presented by Takata and Nagano (12) for single rows and pairs of rows; in it they permit the upstream potential flow to be unsteady, and make the required numerical calculations. Their assumptions about blade-row losses and pressure rise are quite different from those of the present analysis, and seem quite unsuitable for multistage compressors. Their chief concern was to analyze the nonlinear growth of disturbances into rotating stall of single and double rows.

In the next and concluding part of this report, oscillations will be allowed to interact with the entire characteristic diagram, so that resistance to reverse flow and "unstalling" affect the disturbance pattern.

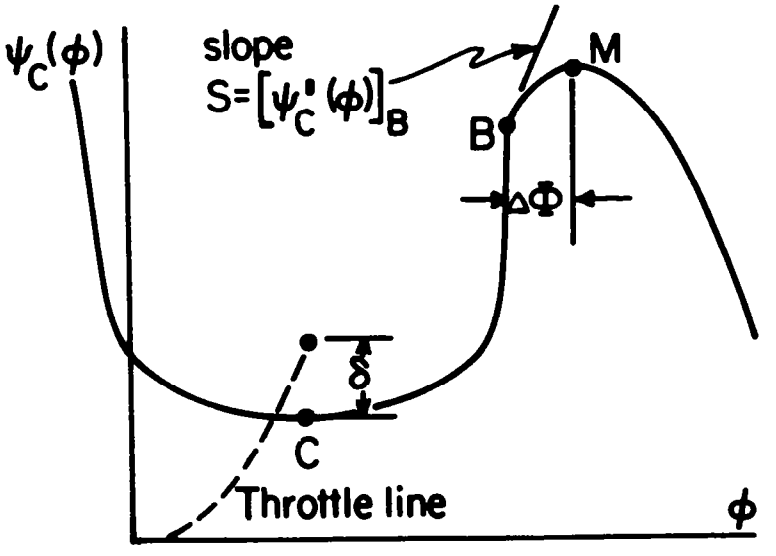

Fig. 2.1. Constant-speed compressor characteristic in the absence of rotating stall.

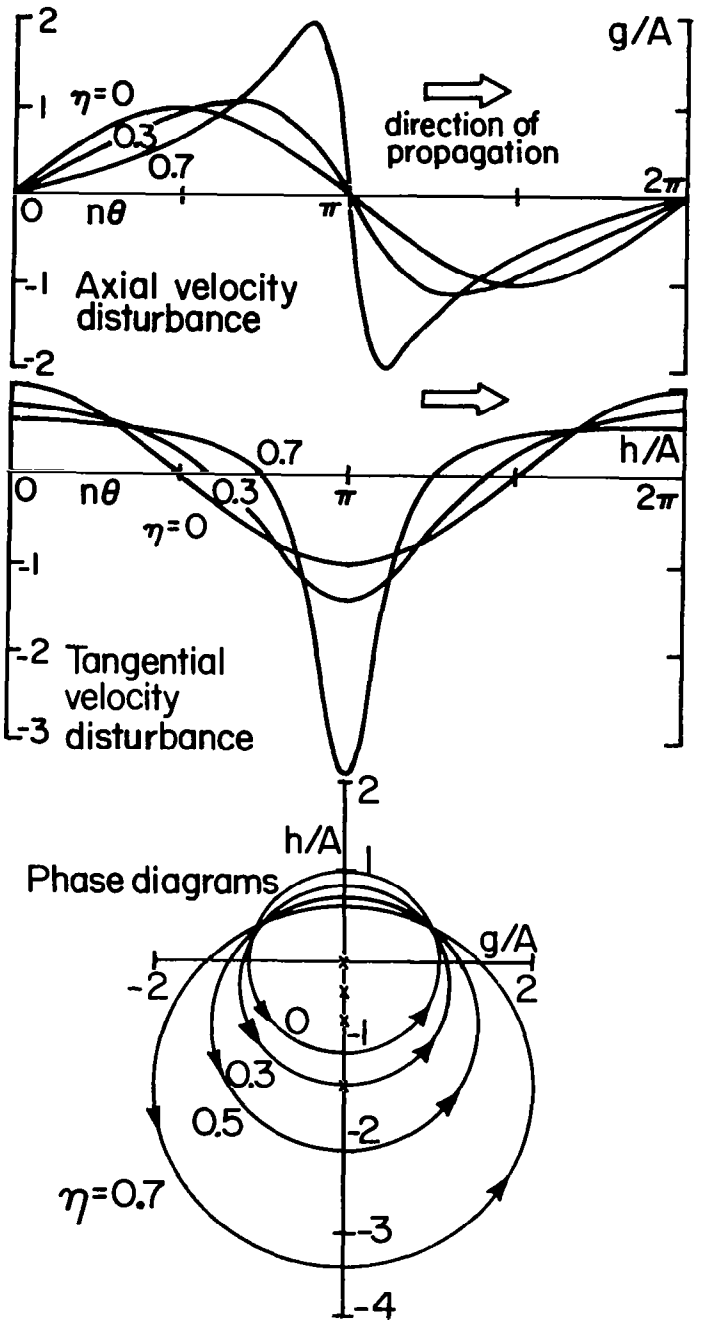

Fig. 2.2. Nonlinear velocity disturbances, for various values of amplitude parameter η, from Eqs. (2.6a,b).

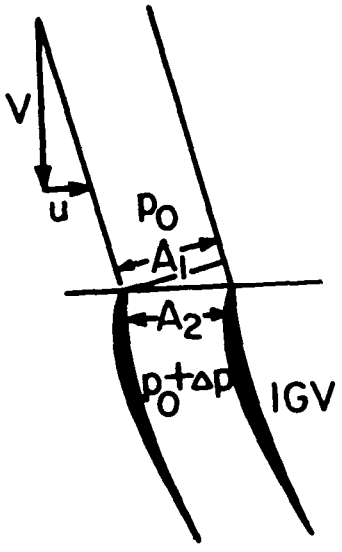

Fig. 2.3. Sketch of the increase of stream-tube area from A_1 to A_2 upon entry into an IGV passage, owing to transverse disturbance velocity u.

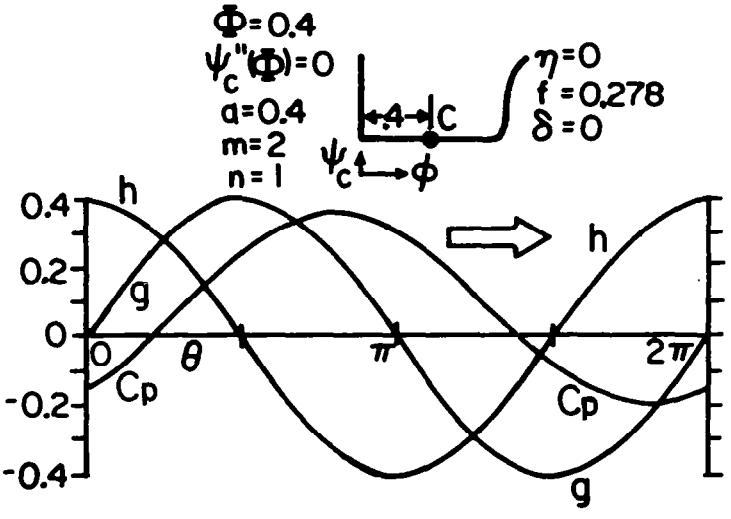

Fig. 2.4. Velocity and pressure disturbances for a flat characteristic ($\psi_c''(\Phi) = 0$) in deep stall. Stall zone is $180 < \theta < 360$ degr, where $g < 0$.

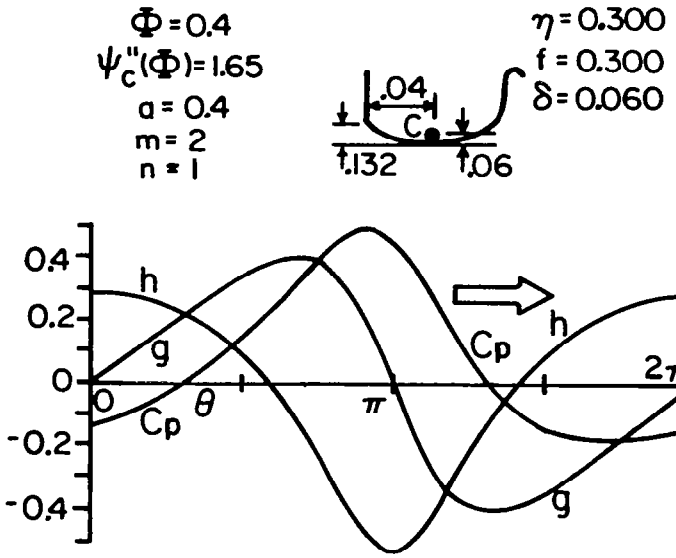

Fig. 2.5. Velocity and pressure disturbances for a concave characteristic ($\psi_c''(\Phi) > 0$) in deep stall. Stall zone is $180 < \theta < 360$ degr, where $g < 0$.

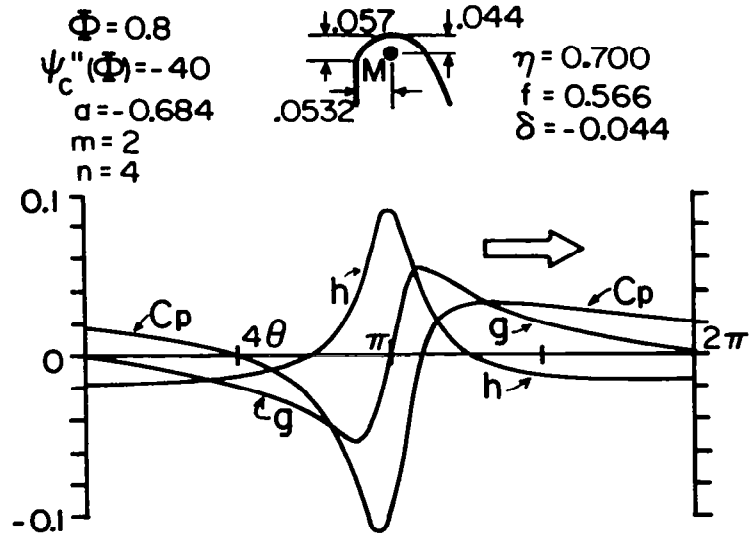

Fig. 2.6. Velocity and pressure disturbances for a convex characteristic ($\psi_c''(\Phi) < 0$) at incipient stall. Note expanded scales. Stall zone is $0 < 4\theta < 180$, where $g < 0$.

PART III - LIMIT CYCLES

SUMMARY

A theory of rotating stall, based on single parameters for blade-passage lag and external-flow lag and a given compressor characteristic yields limit cycles in velocity space. These limit cycles are governed by Liénard's equation with the characteristic playing the role of nonlinear damping function. Cyclic integrals of the solution determine stall propagation speed and the effect of rotating stall on average performance. Solutions with various line-segment characteristics and various throttle settings are found and discussed.

There is generally a limiting flow coefficient beyond which no solution is possible; this probably represents stall recovery. This recovery point is independent of internal compressor lag, but does depend on external lags and on the height-to-width ratio of the diagram. Tall diagrams and small external lags (inlet and diffusor) favor recovery.

Suggestions for future theoretical and experimental research are discussed.

INTRODUCTION

In Part I, it was shown that a simple time lag of blade-passage force, accumulated in a multistage compressor and suitably matched with lags arising in entrance and exit flows, permits rotating stall as a kind of eigensolution of the equations for weak disturbances. A prediction of stall propagation and speed results, and it agrees well with the experiment discussed by Day, Greitzer and Cumpsty (D.G.C.) (3).

In Part II, finite amplitude disturbances were considered in conjunction with compressor characteristics (upstream total to downstream static pressure rise, vs axial flow coefficient) which have parabolic shape over the range of fluctuation. It was found that, if the characteristic diagram is flat, the linear, harmonic solution of Part I applies, presumably limited by resistance to reverse flow. If the diagram is concave the disturbance wave is distorted, with the reduced-flow (stall) zone being steeper at its trailing edge, as observed by D.G.C. If the diagram is convex, as at stall inception, the disturbance is of limited amplitude, especially for multiple-zone stalls when the lag is negative. In this case, propagation speed would exceed 50 percent of wheel speed. These last results may relate to "progressive stall" often observed near the inception point.

None of the foregoing results indicate "recovery"; clearly, a more complete diagram must be used, incorporating unstalled and probably, reversed-flow segments. Use of a more complete diagram should also provide estimates of the effect of the presence of rotating stall on the average compressor performance. This, then, is the theme of this part, to analyze the recovery phenomenon and other results which would come from using a complete performance diagram, and allowing oscillations to enter both unstalled and reverse-flow regions. We will find "limit cycles" which are more complex than the circles in phase space which arose in Parts I and II, and, under certain conditions, these limit cycles will appear to describe "relaxation oscillations", which we will argue represent recovery from rotating stall. Throughout, simple assumptions about internal and external lags will be maintained as in Parts I and II.

THE CYCLE EQUATION

We return to the basic equation (2.1) of Part II. It permits finite amplitude disturbances of axial velocity (g) and transverse velocity (h) at entrance, as functions of angle (θ) around the compressor. Assuming zero entrance loss at the IGV entrance,

$$\lambda g'(\theta) - mfh + \Psi - \psi_c(\phi) = 0. \tag{3.1}$$

Lags are embodied in the parameters λ and mf, where f is propagation speed coefficient, and m reflects inlet and outlet flow lags; if the exit flow is a sudden expansion, and entrance flow is potential, then $n = 1$. If the exit is a straight duct, then we know only that $m = 2$ for small disturbances as well, with $m = 2$ being appropriate for compressors followed by long diffusers. Research is needed to give a more complete picture of exit lag effects. Here, we will show the importance of m, or the phenomena it imperfectly represents, for rotating stall. The compressor lag is embodied in the parameter λ, also related to f according to Eq. (3.16) to follow.

The last two terms of Eq. (3.1) refer to the compressor diagram, sketched in Fig. 3.1. To define $\psi_c(\phi)$, we imagine a test in which ϕ is varied from design to reverse flow, but rotating stall is suppressed by forcing axial velocity to remain circumferentially uniform (a high-drag screen at exit would work, in principle). In that case, ψ_c would be the characteristic measured in the absence of rotating stall. An operating point of the compressor (with axial velocity no longer constrained to be constant) would lie on a throttle line, but at Ψ, either above or below the characteristic. Thus, δ represents the effect of rotating stall on performance at a given average flow coefficient

$\phi = \Phi$. It will be convenient to define the characteristic function relative to the intersection of $\psi_c(\phi)$ and $\phi = \Phi$. Thus,

$$\Psi - \psi_c(0) \equiv \delta; \quad \psi_c(\phi) - \psi_c(0) \equiv G(g) \tag{3.2}$$

and Eq. (3.1) becomes

$$\lambda g'(\theta) - mfh - G + \delta = 0. \tag{3.3}$$

This is the equation to be solved in this part.

If one finds the disturbance functions $g(\theta)$ and $h(\theta)$, the disturbance of static-pressure rise through the compressor can be found from Eq. (2.18). Aside from constants, relative to ρU^2 it is

$$C_p = -mfh + \Phi g + \frac{1}{2}(g^2+h^2). \tag{3.4}$$

This formula includes pressure recovery at the IGV entrance.

Relation of h to g

In order to solve Eq. (3.3) it is necessary to connect the functions h and g. If the upstream flow is potential flow in a straight duct, then $h(\theta)$ is the Hilbert Transform of $g(\theta)$, given for periodic functions by Eq. (1.17):

$$h = -\frac{1}{\pi}\int_0^{2\pi} g'(\xi)\ln\left|\sin\frac{\theta-\xi}{2}\right| d\xi. \tag{3.5}$$

Because g is defined as a difference from average axial velocity, the average $\oint g d\theta = 0$. It can be shown from Eq. (3.5) that it is also true that the average $\oint h d\theta = 0$. Physically, this means that no swirl can be created in the entering potential flow.

Although Eq. (3.5) could be numerically incorporated into Eq. (3.3) (as Takata and Nagano (12) did for their model), it would be desirable to use some simpler relation, such as the one which is valid for single-cell stall and small perturbations, according to Eq. (1.19), with n = 1:

$$h'(\theta) = -g. \tag{3.6}$$

This equation is true for the first terms of Fourier series derivable from Eq. (3.5); in other words, it is exact if g is purely harmonic. Because we are concerned with "deep stall" in this report, for which experiments (3,14) show single-cell stall, we will assume n = 1. Actually, results for higher modes can be inferred by substituting the appropriate multiple of wheel diameter in the parameter a of Eq. (3.16) to follow.

The nonlinear solution, Eq. (2.6b), can be manipulated to yield

$$h' = -(1 - 2\frac{\eta}{A}h)g \tag{3.7}$$

and one could consider making more general use of such a nonlinear relation in Eq. (3.3), rather than Eq. (3.6).

We shall see that a "blockage" function has particular relevance to recovery. That is, $g(\theta)$ might be a step function as shown in Fig. 3.2. The example chosen has a "blockage" of $1-\beta = 20$ percent. Such a "relaxation oscillation" will provide a severe test of the reasonableness of Eq. (3.6). Substitution into Eq. (3.5) gives the corresponding $h(\theta)$:

$$h = \frac{A}{\pi\beta(1-\beta)} \ln \left| \frac{\sin(\frac{\theta}{2} - \pi\beta)}{\sin\frac{\theta}{2}} \right| \tag{3.8}$$

with A being the amplitude of the g-oscillation. Eq. (3.8) is shown on Fig. 3.2; the result is singular at the two values of θ where g jumps. For comparison, we show Eq. (3.6). Apparently, Eq. (3.6) represents the correct Hilbert Transform quite well on the average. Eq. (3.7) would be inappropriate because it would not have the correct anti-symmetry about the midpoints of the stalled and unstalled zones. We are therefore emboldened to adopt Eq. (3.6) for general use in Eq. (3.3); it is correct in the small perturbation (harmonic) limit, and has the correct anti-symmetry as well as a reasonable amplitude in the "blockage" limit.

A more complete justification of the use of Eq. (3.6), and a simple improvement which can be applied, is given in Appendix A.

Liénard's Equation

Eq. (3.6) permits the transformation of Eq. (3.3) into a generalization of the classical van der Pol equation (10), with the characteristic function G(g) playing the role of damping function. From Eq. (3.6),

$$g'(\theta) = - g\, dg/dh. \tag{3.9}$$

In phase space, Eq. (3.3) becomes

$$\lambda g g'(h) + mfh + G - \delta = 0. \tag{3.10}$$

The following transformations and shift or origin (and sign) of h

$$\left.\begin{aligned} \hat{G} &= \frac{G(g)}{(mf)^2}; \quad \hat{\delta} \equiv \frac{\delta}{(mf)^2} \\ \hat{h} &\equiv - \frac{h}{mf} + \hat{\delta}; \quad \hat{g} \equiv \frac{1}{mf}\sqrt{\frac{\lambda}{mf}}\, g \end{aligned}\right\} \tag{3.11}$$

yield a new expression for angle θ,

$$d\theta = - \frac{dh}{g} = \sqrt{\frac{\lambda}{mf}} \quad \frac{d\hat{h}}{\hat{g}} \tag{3.12}$$

and yield the Liénard Equation (10):

$$\hat{g}\hat{g}'(\hat{h}) + \hat{h} = \hat{G}(\hat{g}). \tag{3.13}$$

Eq. (3.12) provides, for a complete cycle,

$$\oint \frac{d\hat{h}}{\hat{g}} = 2\pi\sqrt{\frac{mf}{\lambda}} \tag{3.14}$$

and the requirement $\oint h d\theta = 0$, where Eqs. (3.11) and (3.12) are used, becomes

$$\oint \frac{\hat{h} d\hat{h}}{g} = (2\pi\sqrt{\frac{mf}{\lambda}})\, \hat{\delta}\,. \tag{3.15}$$

If $\hat{G}$ were given, Eq. (3.13) could be solved, and mf/λ found from Eq. (3.14). However, λ and f are related (Eq. (2.7), neglecting effect

of guide vanes for present purposes) by the definition

$$\lambda \equiv \frac{1}{a}\left(\frac{1}{2} - f\right); \quad a \equiv D/(2UN\tau) \tag{3.16}$$

where a is a reciprocal compressor time lag, in effect (Eq. (2.16)). Therefore, f itself can be found. Then, the characteristic displacement $\hat{\delta}$ (or δ) comes from Eq. (3.15). Actually, of course, G(g) would normally be given, rather than $\hat{G}(\hat{g})$, and therefore Eqs. (3.13) and (3.14) would have to be solved simultaneously.

Under the foregoing transformations, Eq. (3.4) becomes

$$C_p = (mf)^2(\hat{h}-\hat{\delta}) + \Phi mf\sqrt{\frac{mf}{\lambda}}\,\hat{g} + \frac{(mf)^3}{2\lambda}\left[\hat{g}^2 + \frac{\lambda}{mf}(\hat{h}-\hat{\delta})^2\right]. \tag{3.17}$$

Fig. 3.3 sketches the usual geometrical construction for solving Liénard's equation (10). The characteristic is reoriented (compare Fig. 3.1) to correspond to the classical damping function. Hereafter, in discussing solutions of Eq. (3.13), we will use this convention without further comment. At a point ⓐ during an oscillation, where the values $\hat{h}$ and $\hat{g}$ apply, one locates point ⓑ, so that the line ⓐ - ⓑ has a length $\hat{h}-\hat{G}(\hat{g})$. The line ⓑ - ⓒ has the length $\hat{g}$. The negative reciprocal of the ratio of these lengths is, by Eq. (3.13), just $\hat{g}'(\hat{h})$ or the slope of the trajectory of the oscillation. Thus, that trajectory is locally perpendicular to the line ⓐ - ⓒ, as sketched in Fig. 3.3. This geometrical method gives a quick sense of the progress of any oscillation in phase space.

Line-Segment Characteristic

In the rest of this paper, we will consider the function G to be various special cases of the line-segment diagram shown in Fig. 3.4a. The quantities $\mathbb{B}$ - $\mathbb{F}$ are parameters of the diagram to be specified. The throttle setting is specified by β. We would usually consider the origin of ϕ to be at $\beta = 0$, so $\beta\mathbb{B} = \Phi$.

A particularly simple but nontrivial case is sketched in Fig. 3.4b. It is a "vertical" diagram in which the unstalled leg is vertical ($\mathbb{D} = 0$) as is the reverse-flow leg ($\mathbb{E} = 0$). The deep-stall leg is horizontal ($\mathbb{C} = 0$). The circular arcs shown dashed in the sketch will be discussed later.

SOME LIMIT-CYCLE EXAMPLES

For purposes of illustration, we first pose a series of "indirect" problems, in which we specify $\hat{G}(\hat{g})$, find the resulting oscillation, determine f, and then infer the function G(g). We note that Eqs. (3.13-15) are invariant to a uniform change of scale. Thus, for example, we may imagine our diagram of $\hat{G}$ to be scaled so that its width is exactly 1; in other words, so that $\hat{g} = g/\mathbb{B}$. On this basis, we assume our diagrams of G to have width 1, with the scale of $\hat{h}$ suitably adjusted. Fig. 3.5 shows a particular choice of diagram shape, double carets signifying the scale adjustment just discussed.

1. Suppose $\beta = 0.5$, and an oscillation begins at a point such as P. An analytic solution of Eq. (3.13) can easily be found for any part of an oscillation for which $\hat{G}(g)$ is a straight line, and these solutions can be pieced together to form a continuous trajectory in phase space. In this case, the trajectory is at first a growing spiral (the construction of Fig. 3.3 suggests this result directly) which grows until it encounters reverse-flow resistance, and then becomes momentarily "unstalled." After about three circuits, the oscillation becomes self-duplicating; that is, a "limit cycle" of the sort familiar in nonlinear mechanics, and in fact which is classically illustrated by Liénard's equation with an S-shaped damping function. The usual compressor diagram, when properly oriented, is of that classical shape.

The initial amplification in this example is due to the deep-stall slope being positive. If it were negative, the oscillation would locally damp. In any case, the peak of $\hat{G}$ being to the right of the reverse-flow corner is amplifying, for an oscillation which is already strong enough. The slopes of unstalled and reverse-flow legs being negative and (locally) limiting. Thus, the oscillation, as it grows, ultimately settles into a limit cycle.

2. The limit cycle depends on the throttle setting (β) for a given diagram. Fig. 3.6 shows the effect. Various symbols on the cycle traces serve to relate each trace to the value of β indicated in the legend and along the deep-stall line where each cycle is centered. It is noteworthy that if β is somewhat less than 0.5, the cycle is "caught" by the reverse-flow leg. As β approaches 1, the "release point" moves closer to the maximum-$\hat{G}$ corner, and, in fact, the unstalled part of the cycle tends to hug the unstalled leg of the diagram. If β is slightly greater than 1, the unstalled leg actually catches the trajectory before it reaches the corner, and a rapidly damped oscillation follows (because the unstalled leg has negative slope).

Table 3.1 shows the results when Eqs. (3.14) and (3.15) are used to find f and hence G(g) and δ. We assume $m = 2$, and $a = 1$, in order to make the example definite. The actual $\mathbb{F}$ is only about 43 percent of $\mathbb{B}$;

rather a lightly-loaded compressor. The value of f is about 0.26, tending to increase as β increases. As is obvious from Fig. 3.6, the δ needed to bring the average h to zero is greatest when $\beta = 0.5$; that cycle lies more to the right than the others.

Fig. 3.7 shows the profiles of $g(\theta)$ which may be derived from Fig. 3.6 and Eq. (3.12). The wave is propagating to the right. Thus, the fraction of circumference with reduced flow becomes less as β increases, as one would expect. There is a tendency, not very strong, for the "trailing edge" of the reduced-flow (stall) zone to be steeper than the leading edge, for the lower flow rates, as observed by D.G.C. (3).

3. The limit cycle depends on the diagram "tallness." Fig. 3.8 shows how the limit cycle changes when β is kept at 0.9, but the scale of $\hat{G}$ is changed by factors of 2 and 3 beyond the case shown in Fig. 3.6 (and repeated in Fig. 3.8 for comparison). Obviously, as scale of $\hat{G}$ increases, the cycle follows the unstalled leg very closely indeed, releasing just at the top point of the diagram in the limit. The reverse-flow leg is also followed closely, and, again, release occurs close to the lower corner of the diagram. These effects of diagram tallness will be of great significance in our subsequent discussion of recovery.

The last three rows of Table 3.1 show the completed calculations. Even in the most extreme case, $\mathbb{F}$ is only about equal to $\mathbb{B}$. In that case, f has increased to 0.43, and δ has increased dramatically, as Fig. 3.8 suggests it should.

Fig. 3.9 shows $g(\theta)$ for the most extreme case, to be compared with the profile $\beta = 0.9$ in Fig. 3.7. The stalled angle is reduced, and the expected steepness of the stall trailing edge is very definite. The intercepts of a horizontal line ($\hat{G} = 0$) with the unstalled and reversed legs are shown (unstall g" and "reverse g") to indicate how well this profile conforms to blockage ideas, namely that the flow is either stalled or unstalled. The concept seems not to be very useful in this case. Also shown is the pressure-rise disturbance C_p, obtained from Eq. (3.17), with $\mathbb{B}$ taken to be 1.

We proceed now to analysis of the direct problem, in which a simple "vertical" shape of G(g) is given, and we will pay particular attention to indications of stall recovery as the throttle is opened.

IDEAL-DIAGRAM SOLUTIONS

Vertical Diagram

The "vertical" diagram of Fig. 3.4(b) has only $\mathbb{F}$ and $\mathbb{B}$ as parameters, and, because the equations are invariant to overall scale change, only the single parameter $\mathbb{F}/\mathbb{B}$ is significant, along with throttle setting β.

The limit cycle in this case is simply described in the $\hat{h},\hat{g}$ plane. Reference may be made to Fig. 3.4(b), imagining it to be transformed to $\hat{h}$ and $\hat{g}$, or as if mf = 1. Eq. (3.13) tells us that the cycle follows the unstalled leg ($\hat{g}' = 0$) until the peak of $\mathbb{F}$ is reached ($\hat{h} = \hat{G}_{max}$). The cycle leaves that corner, and is governed by $\hat{G}(\hat{g}) = 0$. In that part of the cycle, Eq. (3.13) is satisfied by a circular arc centered at (0,0). It is shown dashed on Fig. 3.4(b). The arc will intersect the reverse-flow leg as shown, provided the diagram is tall enough.

In the $\hat{h},\hat{g}$ plane, "tallness" will depend on f as well as $\mathbb{F}/\mathbb{B}$, because of the transformations, Eqs. (3.11) and (3.12). The height-to-width ratio will be

$$\frac{\mathbb{F}/\mathbb{B}}{\sqrt{\lambda mf}}$$

in the $\hat{h},\hat{g}$ plane. Thus, if f is near 0.5, so that λ is small, then any diagram will be "tall" in the $\hat{h},\hat{g}$ plane, and, incidentally, the cycle will always reach the reverse-flow line.

The cycle will then follow the reverse flow line until the corner is reached at $\hat{h} = 0$. Then another circular arc governs the return to the unstalled condition. This second arc will reach the unstalled line only if $\beta > 0.5$. If $\beta < 0.5$, the arc will simply complete a circle back to the starting point. This solution corresponds to the purely harmonic wave (limited by reverse-flow resistance) discussed in Part II.

It is a simple matter to evaluate the cyclic integrals, Eqs. (3.14) and (3.15) in these cases. Along the arc segments, the differential $d\hat{h}/\hat{g}$ is simply the angle increment along the arc. Therefore, according to Eq. (3.12), the real angle change, $d\theta$, is simply $\sqrt{\lambda/mf}$ times the angle of arc in the $\hat{h},\hat{g}$ plane. An immediate conclusion may be drawn: Fig. 3.4(b) shows that the arc from unstalled to reverse condition generally subtends a smaller angle than the return. Therefore, the drop into stall is more abrupt than the recovery. Since the stall zone is traveling in the positive θ direction (Fig. 1.4), the drop into stall is the "trailing edge" of the stall zone, in D.G.C.'s terminology (3), and, in keeping with their observations, the trailing edge of the zone is predicted always to be steeper than the "leading edge."

The foregoing simple calculations were made for various $\mathbb{F}/\mathbb{B}$, λ, and mf, subject to the requirement of Eqs. (3.14), and finding δ from Eq. (3.15). Typical results are shown for $\mathbb{F}/\mathbb{B} = 1$ on Fig. 3.10. The solid-line results do not depend on compressor lag (a); only when the definition of λ (Eq. (3.16)) is introduced, overlaid on Fig. 3.10 as

dot-dashed lines, does a become a factor. The intersections of dashed and solid lines provide the solution shown in Fig. 3.11 for the special cases of m = 2 and a = 0.3 and 0.6.

These solutions describe two regimes: The harmonic wave, for which $\delta = 0$, when $\beta < 0.5$, and a rather different wave when $\beta > 0.5$. The velocity, pressure-rise, and phase diagrams for these two cases (with a = 0.6) are shown as the first and second rows of Fig. 3.12. The steeper "trailing edge" is evident in $g(\theta)$ for $\beta > 0.5$.

It is obvious from Fig. 3.10 that the external lag parameter (m) is more significant than the internal one, especially for the larger values of β. The speed f is restricted to be less than 0.5. Therefore, if m is small, say 1, rotating-stall solutions might be forbidden entirely. Even if m = 2, no solution is possible when $\beta > 0.801$. In the next paragraphs, this point will be discussed more fully.

The Recovery Limit

When m = 2, a limit is reached when $\beta = 0.801$. At that limit, which is independent of a, the speed f goes to 0.5, and so does $\delta/\mathbb{F}$. The third row of Fig. 3.12 shows the corresponding traces. The axial velocity becomes a pure step wave and the circumferential velocity is a saw tooth. (This type of "relaxation oscillation" was discussed earlier in connection with Fig. 3.2.)

The phase diagram becomes a rectangle because λ has approached zero. From Eq. (3.10) one would expect dg/dh to become infinite when $\lambda \to 0$. Another way to see this result is to recall that the cycle includes arcs in the $\hat{h},\hat{g}$ plane, in which the diagram is infinitely "tall" when $\lambda \to 0$. That is, while g changes by $\mathbb{B}$, Eq. (3.12) says that g changes only to order $\mathbb{B}\sqrt{\lambda}$ when λ is small. Thus, the arcs depart to a vanishing degree from $\hat{h} = \mathbb{F}/(1/2)m$ when stalling or $\hat{h} = 0$ when unstalling. The result in the original frame of reference is a rectangular cycle.

Pursuing further the effort to interpret the limiting solution physically, we may focus attention on Eq. (3.14). Essentially, it is the requirement that the cycle complete itself in the angular distance 2π. Now if we specify a large β, then $\hat{g}$ is a small constant quantity on the unstalled leg of the cycle. The coordinate $\hat{h}$ must change by a certain amount essentially fixed by the height of the diagram ($\mathbb{F}$). Thus, the contribution of the unstalled leg to the integral $\oint d\hat{h}/\hat{g}$ will be of the order $\mathbb{F}/[(1-\beta)\mathbb{B}\sqrt{\lambda}]$, and Eq. (3.14) suggests that if β is too near 1, the unstalled leg will use up all the allowed range of θ. Clearly, β may be permitted to be largest when the other terms of the integral are minimized. This occurs when the stalling and unstalling arcs have the least angle in the $\hat{h},\hat{g}$ plane, namely zero when $\lambda \to 0$, and the negative-$\hat{h}$ portion of the unstalled leg is minimized; again, when $\lambda \to 0$. In the $\lambda \to 0$ limit, the reverse flow leg is longest, but $\hat{g}$ is larger there, and so the contribution to β is less important.

Appendix B provides further physical discussion of the relaxation-cycle limit as a matter of "detailed balancing" of pressure changes in a stage.

In summary, as the throttle is opened, a limiting condition is reached such that the cycle spends too much time unstalled to permit the required pressure changes of stalling and unstalling to occur. This description would seem to fit the phenomenon of "stall recovery" (3). It is significant that δ is quite large (about (1/2)$\mathbb{F}$) when the critical $\beta = \beta_{cr}$ is reached. If this is true, a discontinuity of Ψ is predicted to occur when $\beta = \beta_{cr}$. The geometry of Fig. 3.1 suggests that a slightly more open throttle line than that for β_{cr} would have no nearby performance line to intersect, and a jump across to the unstalled line (i.e., recovery from stall) would have to occur.

The value $\beta_{cr} = 0.801$ applies only for a vertical characteristic with $\mathbb{F}/\mathbb{B} = 1$ and $m = 2$. The general results for a vertical characteristic are

$$\beta_{cr}(1-\beta_{cr}) = \frac{\mathbb{F}/\mathbb{B}}{\pi m} \; ; \quad \frac{\delta_{cr}}{\mathbb{F}} = \frac{1}{2} \tag{3.18}$$

which appear as the lowest curve on Fig. 3.14. If the diagram is less "tall," β_{cr} can approach 1. On the other hand, if $\mathbb{F}/\mathbb{B}$ exceeds $(1/4)\pi m$, no rotating stall other than the harmonic variety can occur.

In general, a tall diagram (large $\mathbb{F}/\mathbb{B}$) and a small value of m favor recovery. The role of m is particularly significant. We have inferred that m is about 2 for a compressor with a straight outlet. If m were reduced to 1 by using a sudden expansion, rotating stall could be largely suppressed, according to the present analysis, when $\mathbb{F}/\mathbb{B}$ is greater than about 0.8. Thus, changes in external lag mechanisms could be very effective for relatively "tall" diagrams, it would seem.

The Step Diagram

Another sort of ideal, simple diagram would continue to have $\mathbb{C} = \mathbb{E} = 0$, but $\mathbb{D} = \infty$ rather than 0. Fig. 3.13(a) shows such a "step" diagram, together with a phase diagram in the $\hat{h},\hat{g}$ plane (as if $mf = 1$). Such an extended unstalled plateau seems a possible model for Iura and Rannie's diagram (13), but is not typical of modern compressors.

The results show a lower, rather than an upper limit for rotating stall. It is

$$\beta_{cr} = 2\,\frac{\mathbb{F}/\mathbb{B}}{\pi m} \tag{3.19}$$

shown in Fig. 3.13(b). If the diagram is tall enough, there is a forbidden gap between $\beta = 0.5$ and β_{cr} where a rotating-stall solution is impossible. This is true only if $\mathbb{F}/\mathbb{B}$ exceeds $(1/4)\pi m$, which is quite tall. For smaller values of $\mathbb{F}/\mathbb{B}$, there is no critical case, and solutions for f are quite far from 0.5. For example, if $\mathbb{F}/\mathbb{B} = 0.5$, $m = 2$, and $a = 0.6$, the speed f would remain in quite a narrow range: 0.35 at $\beta = 0.5$ and 0.25 at $\beta = 1.5$.

RECOVERY FOR LINE-SEGMENT CHARACTERISTIC

We now return to the more general line-segment characteristic shown in Fig. 3.4(a), and look for the effects of nonzero $\mathbb{C}$, $\mathbb{D}$, and $\mathbb{E}$. The general solution is easy to find, but hard to discuss because there are so many parameters to consider; the previous section describing Figs. 3.6-9 will suffice for illustration. If we consider only recovery, simplifications are available; f approaches 0.5, λ approaches 0, and compressor lag (a) becomes irrelevant.

As $\lambda \to 0$, we have seen how the transformation Eq. (3.12) makes the diagram "taller" in the $\hat{h},\hat{g}$ plane without limit, so that, as in the vertical diagram case, the unstalling and stalling legs are lines of constant $\hat{h}$. The deep-stall slope $\mathbb{C}$ becomes irrelevant except in finding δ, provided $\mathbb{C}$ is positive. If $\mathbb{C}$ is negative, the cycle would presumably follow the deep-stall leg and release at the corner $g = (1-\beta)\mathbb{B}$. We do not consider this possibility any further in the present paper. With $\mathbb{C} > 0$, the only change from the vertical-diagram analysis is that the integral of $d\hat{h}/\hat{g}$ must be carried out along the slanted lines defined by $\mathbb{D}$ and $\mathbb{E}$. When this is done, the following formulas for recovery result:

$$\frac{\mathbb{F}/\mathbb{B}}{\pi m} = 1/\ln\left[\left(1 + \frac{\mathbb{D}/\mathbb{B}}{1-\beta_{cr}}\right)^{\mathbb{B}/\mathbb{D}}\left(1 + \frac{\mathbb{E}/\mathbb{B}}{\beta_{cr}}\right)^{\mathbb{B}/\mathbb{E}}\right] \tag{3.20}$$

$$\frac{\delta_{cr}}{\mathbb{F}} = \frac{\mathbb{F}/\mathbb{B}}{\pi m}\left[\frac{1 - \beta_{cr} + \mathbb{D}/\mathbb{B}}{(\mathbb{D}/\mathbb{B})^2}\ln\left(1 + \frac{\mathbb{D}/\mathbb{B}}{1-\beta_{cr}}\right) - \frac{\mathbb{B}}{\mathbb{D}}\right.$$

$$\left. + \frac{\beta_{cr} + \mathbb{E}/\mathbb{B}}{(\mathbb{E}/\mathbb{B})^2}\ln\left(1 + \frac{\mathbb{E}/\mathbb{B}}{\beta_{cr}}\right) - \frac{\mathbb{B}}{\mathbb{E}}\right]. \tag{3.21}$$

These formulas reduce to Eq. (3.18) when $\mathbb{E}$ and $\mathbb{D}$ are set equal to zero. The formula for δ is valid even if $\mathbb{C}$ is not zero, so long as δ is measured from the reverse-flow corner at $g = -\beta\mathbb{B}$.

Fig. 3.14 shows the effect of "slant," choosing $\mathbb{D} = \mathbb{E}$ for convenience. Clearly, slant increases the value of β_{cr}; in other words, it delays recovery. It remains true, however, that a tall diagram with small m will favor recovery. Fig. 3.14 shows how the maximum value of $\mathbb{F}/m\mathbb{B}$, which occurs at $\beta_{cr} = 0.5$, depends on the slant parameter $\mathbb{D}/\mathbb{B}$. The more slanted the characteristic, the taller may be the diagram before the rotating-stall limit descends to $\beta_{cr} = 0.5$. Fig. 3.14 also suggests that for realistic slants of about 0.5, recovery occurs in a fairly narrow range of β (between 0.9 and 1.0 for $\mathbb{F}/\mathbb{B} < 0.7m$). In D.G.C. (3), it is suggested that experiments indicate recovery when a certain critical blockage (about 0.7) occurs. The present analysis is not quite consistent with this idea because β_{cr} is not the same as blockage. If β_{cr} is near 1, and $\mathbb{D}/\mathbb{B} = 0.4$, then the two ideas do happen to agree.

The dashed lines of Fig. 3.14 show that δ_{cr} is not greatly affected by slant unless β_{cr} is quite near 1. Of course, that is the region where recovery is generally predicted.

Further results of Eqs. (3.20,21) are provided in Appendix C, together with a set of recovery predictions which emphasize that only the top and bottom points of the diagram are needed to fix the relaxation-cycle limit.

COMPARISON WITH EXPERIMENT

Comparison of the present theory with experiment is handicapped by ignorance of the rotating-stall-free characteristic $\psi_c(\phi)$. In principle, it could be measured, but heretofore there has not been sufficient reason to do so. Nevertheless, in Part I it was shown that theoretical predictions of propagation speed (f) agreed well with experiment. Here, we are concerned chiefly with recovery, and we may appeal to D.G.C. (3) for evidence.

Recovery

Fig. 3.15 shows characteristics measured and reported by D.G.C. These appear as solid lines, with the recovery point indicated by a circle. Three different loadings are included, all at 50 percent reaction. For theoretical predictions, we have assumed that the shut-off head describes a constant value of deep-stall ψ_c, and calculated values of δ are applied relative to that level of ψ_c.

Therefore, if vertical diagrams were used, the theory would follow the dashed lines shown in each of the three cases. The average slant of the unstalled leg gives a basis for estimating the recovery point by use of Eqs. (3.20) and (3.21). These points are triangles, and are presumably better estimates than the diamonds which terminate the vertical-characteristic results.

The "low-ϕ*" (Case I) results are not very informative. The "intermediate-ϕ*" (Case II) results show excellent agreement, even including a suggestion of transition from harmonic to limit-cycle waves. The "high-ϕ*" (Case IV) is reasonable as regards β_{cr}, but quite poor as regards vertical shift of Ψ. Probably, the slope $\mathbb{C}$ of the deep-stall ψ_c should be taken as negative. If so, the integral $\oint d\hat{h}/\hat{g}$ should be recalculated. It seems doubtful, however, that such a revision would give such a low value of Ψ at recovery. Perhaps the throttle plays a special role in recovery when the characteristic descends to such a low limit.

In all cases, it is worth noting that recovery, both in theory and experiment, is close to the breakpoint of the characteristic. That is, $\beta \approx 0.95$ at recovery. Perhaps this may prove a more basic concept than blockage.

Propagation Speed

Fig. 3.16 shows the propagation speeds which correspond to the Cases I, II, and IV of Fig. 3.15. These speeds, given in Day's Thesis (14), relate to theory just as recovery does in Fig. 3.15, if we recall that f should approach 0.5 ($\lambda \to 0$) at recovery, according to Fig. 3.11.

The low-ϕ* Case I does not show the predicted rise of f toward 0.5, but the measurements do not extend to recovery; perhaps the rise would indeed occur if recovery were more closely approached.

The intermediate-ϕ* Case II does show the predicted rise; perhaps the good agreement in this case is related to the good agreement of recovery prediction and experiment shown for Case II in Fig. 3.15. The high-ϕ* Case IV shows the least agreement; the experiments show no rise, all the way up to recovery.

Iura and Rannie (13) also report a propagation speed which remains nearly constant right up to recovery. In their experiments, the compressor has an extended plateau of pressure beyond the stall point, somewhat like the steep characteristic of Fig. 13. In that case, we would in fact predict a nearly flat value of f.

Further comparisons of theory with experiment will require, on the one hand, a more thorough theoretical exploration of the parameters of the problem, and on the other hand, new measurements of rotating-stall-free compressor characteristic maps.

CONCLUDING REMARKS

The problem of rotating stall has been difficult largely because it occurs in such a complex parameter space. Perhaps the best service theory can provide in such a situation is to suggest priorities among these parameters, rather than to predict the resulting phenomenon in detail. The present set of three reports is set forth in this spirit. The most important results seem to be the following:

1. The recovery from rotating stall seems basically predictable. It depends on the compressor's steady characteristic; primarily its "tallness" (the height of the drop into stall compared with the diagram width), and secondarily the slope of the unstalled characteristic. Tallness favors early recovery. The slope of the reverse-flow resistance is of minor significance, as is the slope of the deep stall line, provided that slope is positive. If it is negative, the throttle curve may be important; otherwise, the throttle characteristic is unimportant.

Recovery does not depend on compressor lag (dynamic hysteresis), but it depends very much on the lags originating in the entrance and exit flows. Small external lags favor recovery. It seems likely that the most directly effective design change would be to reduce the lag in the exit duct. Appendix D provides a brief analysis which indicates that a converging entrance would provide a reduced external lag (smaller value of m) also.

2. The characteristic with rotating stall suppressed must be found experimentally to form a proper basis for further theoretical refinements. Discharge to a very low pressure through a dense screen at exit would force circumferentially uniform axial flow, and suppress rotating stall. Also, it would be important to suppress any effects of finite throttle-line slope, such as steady hysteresis about stall. Again, discharge to a low pressure would tend to steepen the throttle lines in the necessary way.

3. Research is needed on entrance flow fields and, especially, diffusers with transversely non-uniform flow. Dynamic (lag) effects are very important, more so than compressor blade-row dynamics.

4. Theoretical limit-cycle analysis can easily be extended to include a wider class of hypothetical characteristic diagrams, and a certain "exact" entrance and exit-flow relation. It is felt that these should proceed in parallel with the studies discussed in 2 and 3 above.

Appendix E contains more detailed discussions of the implications of the theory of this report for future experimental, theoretical and computational research.

TABLE 3.1. RESULTS FOR LIMIT-CYCLE EXAMPLES

Shapes of $\hat{G}(g)$, as in Figs. 3.5 and 3.8, defined by reference to Fig. 3.4: $\hat{B} = 1$; $\hat{D} = \hat{E} = 9/16$; $\hat{F} = 0.9$; $\hat{C} = 0.2$. In Fig. 3.8, $\hat{F}$ and $\hat{C}$ multiplied by 1, 2, 3. m = 2, a = 1.

Symbol	β	$\sqrt{\frac{mf}{\lambda}}$	$\hat{\delta}$	f	$\sqrt{\lambda mf}$	F/B	δ/F
△	0.25	1.028	0.043	0.26	0.50	0.45	0.048
o	0.50	1.076	0.221	0.26	0.60	0.45	0.246
□	0.75	1.084	0.190	0.26	0.50	0.45	0.121
◇	0.90	1.151	-0.032	0.29	0.50	0.45	-0.036
▽	1.00	1.336	0.068	0.32	0.48	0.43	0.076
◇	0.90	1.151	-0.032	0.28	0.50	0.45	-0.036
⬭	0.90	1.178	0.387	0.37	0.44	0.78	0.215
▢	0.90	2.400	0.766	0.426	0.36	0.96	0.284

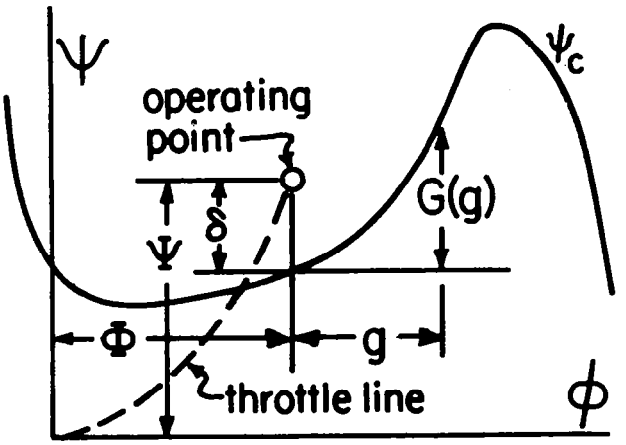

Fig. 3.1. Sketch of notation on compressor performance diagram, of total-to-static pressure rise (ψ_c) vs flow coefficient (ϕ) in absence of rotating stall. Operating point in rotating stall is δ above steady diagram.

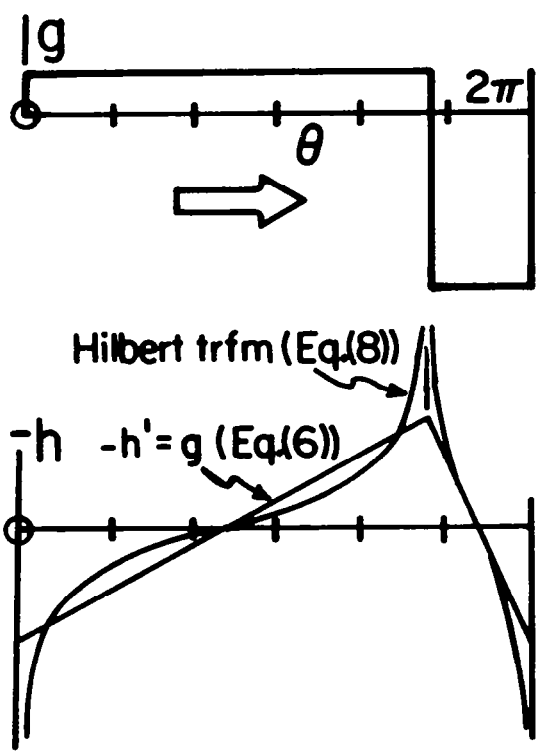

Fig. 3.2. Comparison of correct determination of h from g (Eq. (3.8)) with generally approximate Eq. (3.6), for a step wave ($\beta = 0.8$).

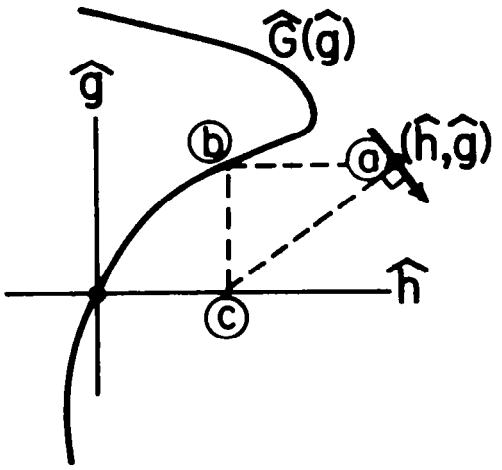

Fig. 3.3. Geometrical solution of the Liénard Equation (Eq. (3.13)).

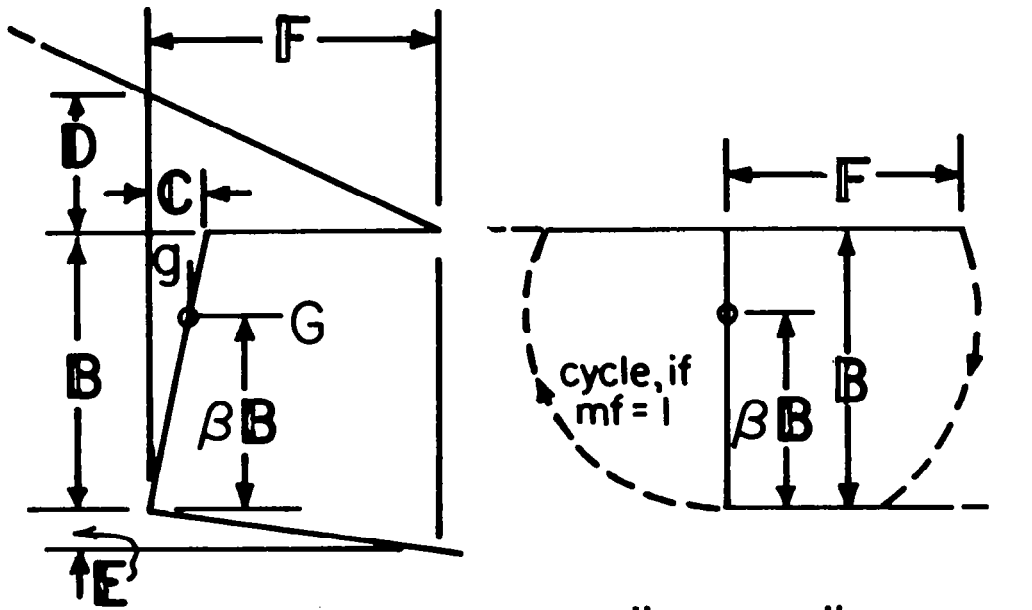

Fig. 3.4. Line-segment characteristic diagrams, of function G(g), oriented as in Fig. 3.3.

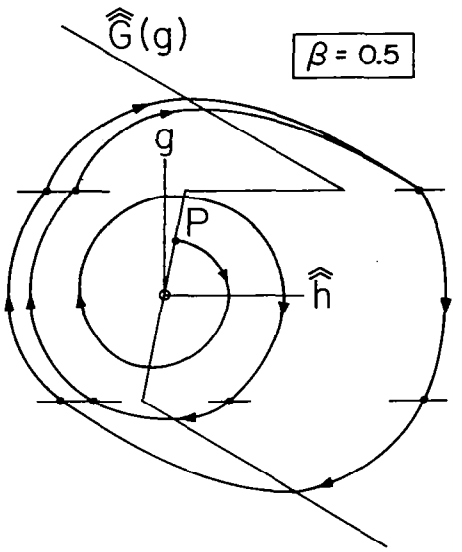

Fig. 3.5. Development of limit cycle, for $\beta = 0.5$. Oscillation begins at point P. After three cycles, negligible changes. See Table 3.1 for diagram parameters corresponding to assumed $\hat{G}(g)$.

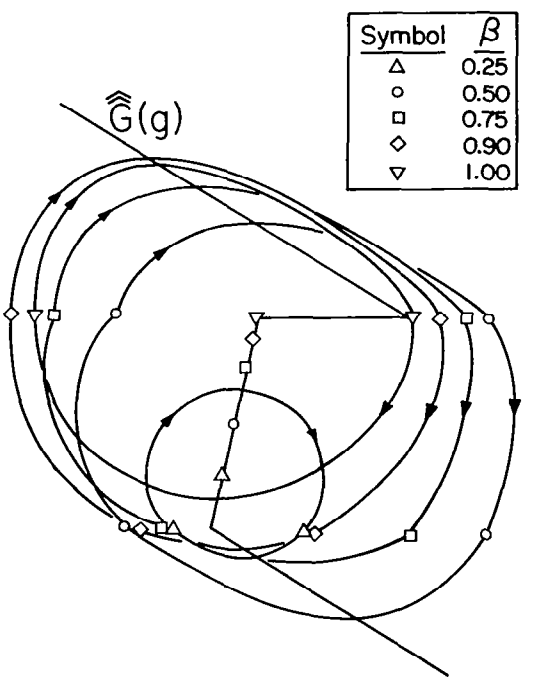

Fig. 3.6. Effect of throttle setting (β) on limit cycles; for the same given $\hat{G}(g)$. See Table 3.1 for the corresponding diagram parameters.

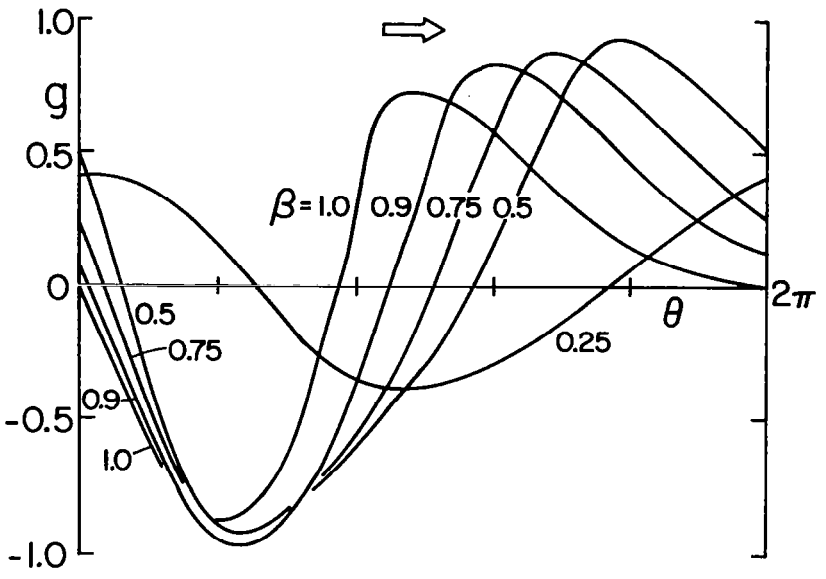

Fig. 3.7. Axial-velocity disturbance around the compressor, for the various throttle settings given in Fig. 3.6. Here, $\mathbb{B} = 1$.

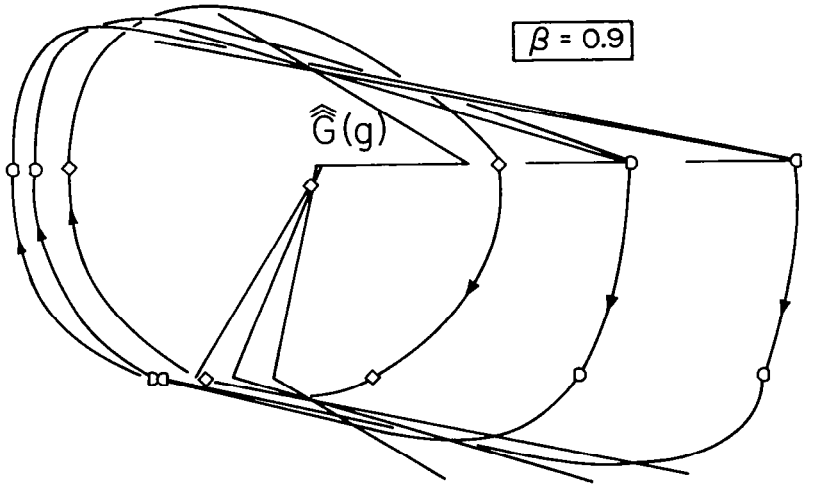

Fig. 3.8. Effect of changes of diagram height (scale of $\hat{G}$). See Table 3.1 for the numerical values.

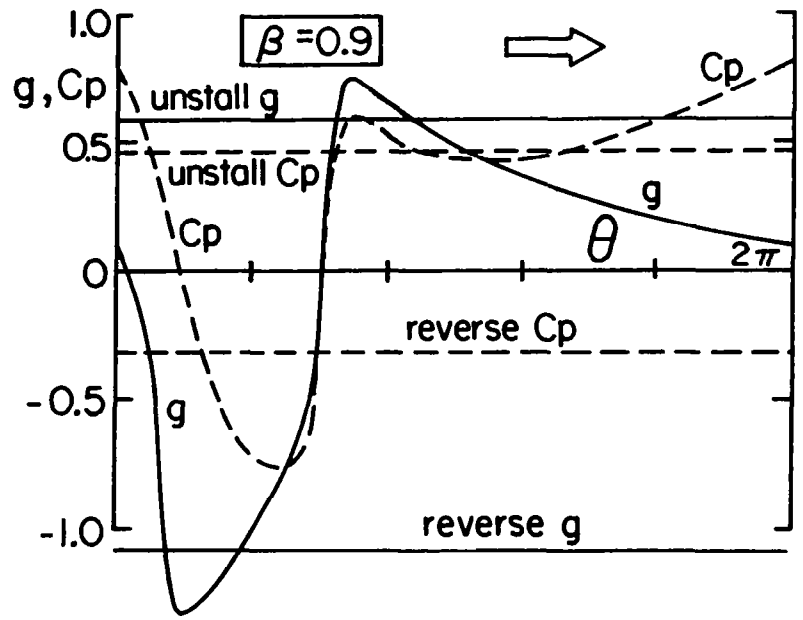

Fig. 3.9. Axial velocity (g), static pressure-rise (C_p) disturbances, for $\beta = 0.9$ and the most extreme case of Fig. 3.8 (Symbol ○, see Table 3.1).

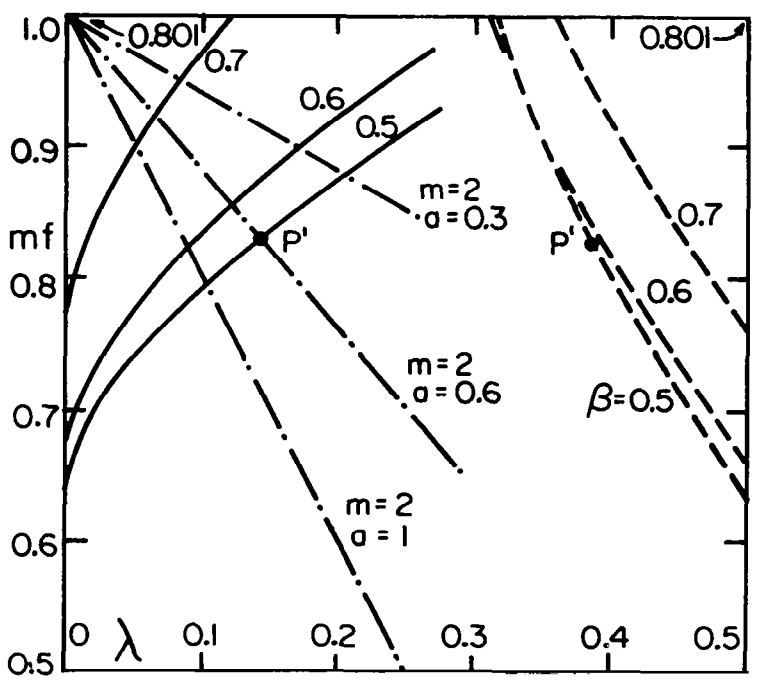

Fig. 3.10. λ and δ (shown dashed) vs mf for various β and $\mathbb{F}/\mathbb{B} = 1$. The definition of $\lambda \equiv (1/a)[(1/2)-f]$ overlaid (dot-dashed). Point P' gives the solution for $\beta = 0.5$ when $a = 0.6$, $m = 2$.

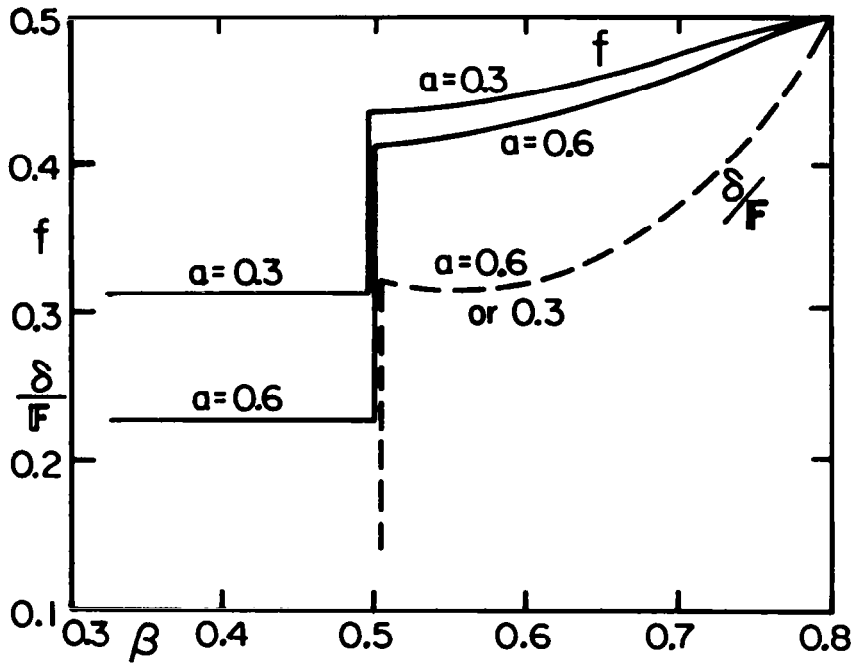

Fig. 3.11. Propagation speed (f) and performance rise due to rotating stall (δ) shown dashed vs throttle setting (β), for m = 2 and $\mathbb{F}/\mathbb{B}$ = 1. No solution for m = 1. Note that β_{cr} = 0.801 is independent of lag (a), and that δ = 0 for $\beta < 0.5$.

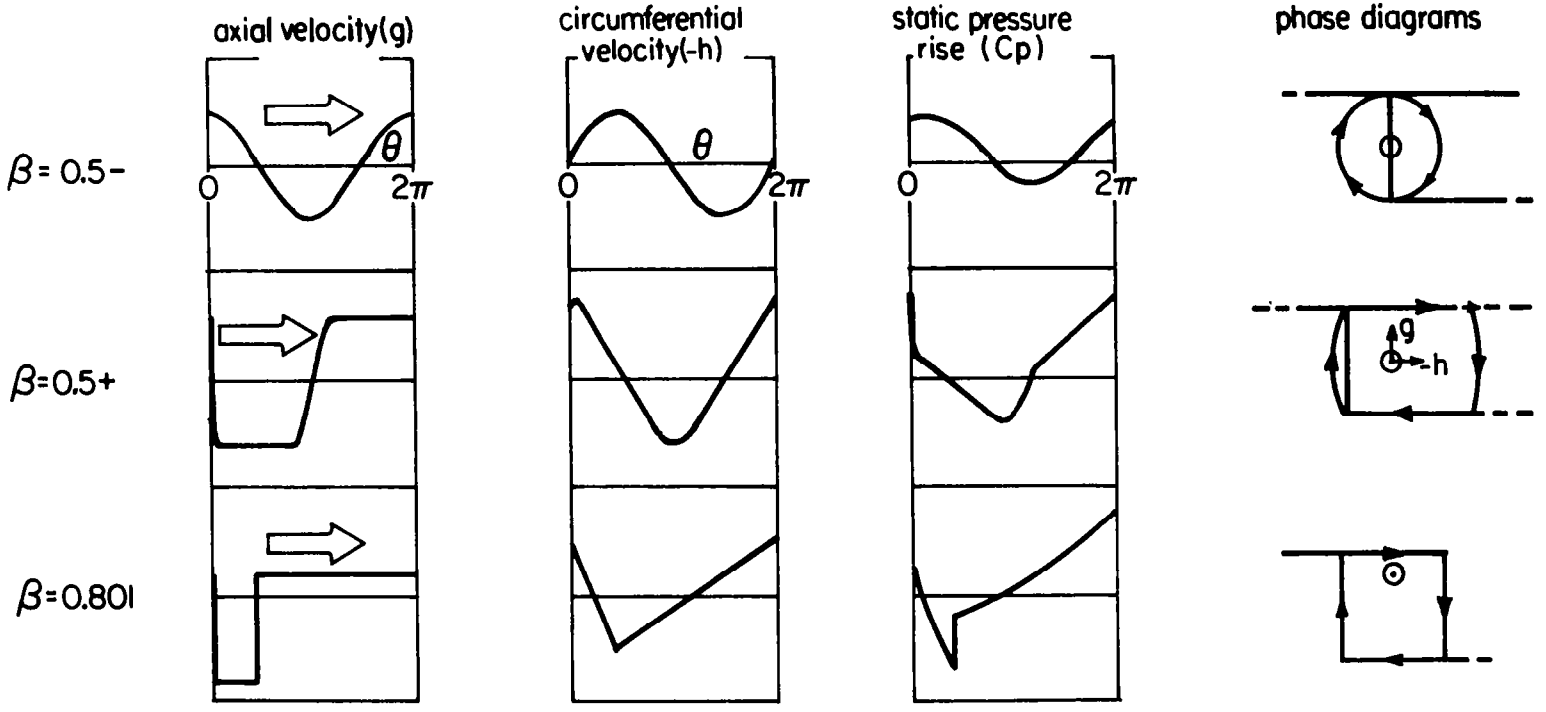

Fig. 3.12. Theoretical velocity and pressure "traces" and phase diagrams, for a particular vertical characteristic, and three values of β (β_{cr} = 0.801), m = 2, a = 0.6. Arrow denotes direction of propagation.

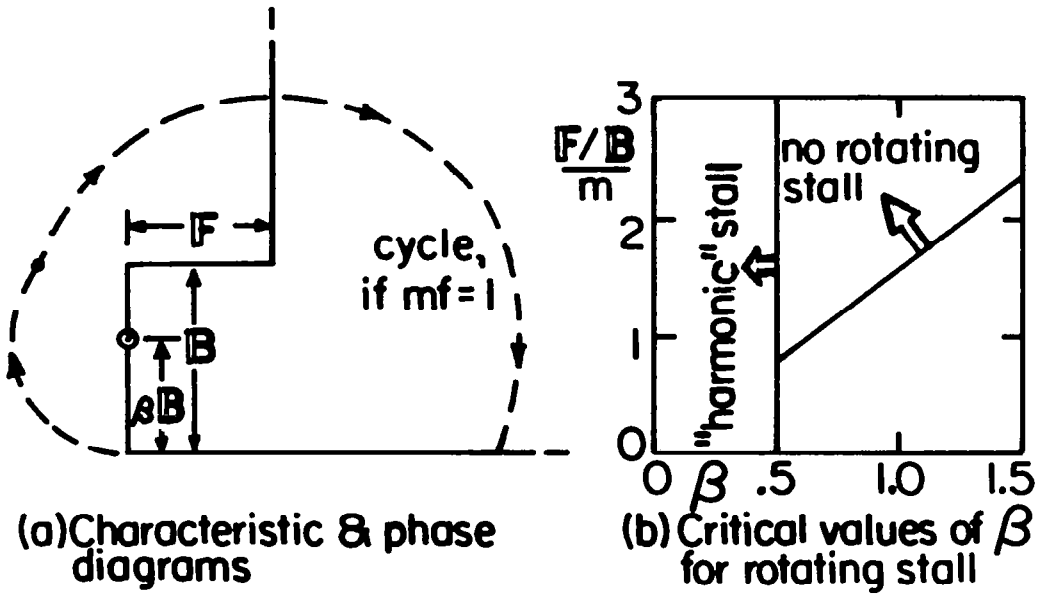

Fig. 3.13. Results for step-type characteristic, m = 2.

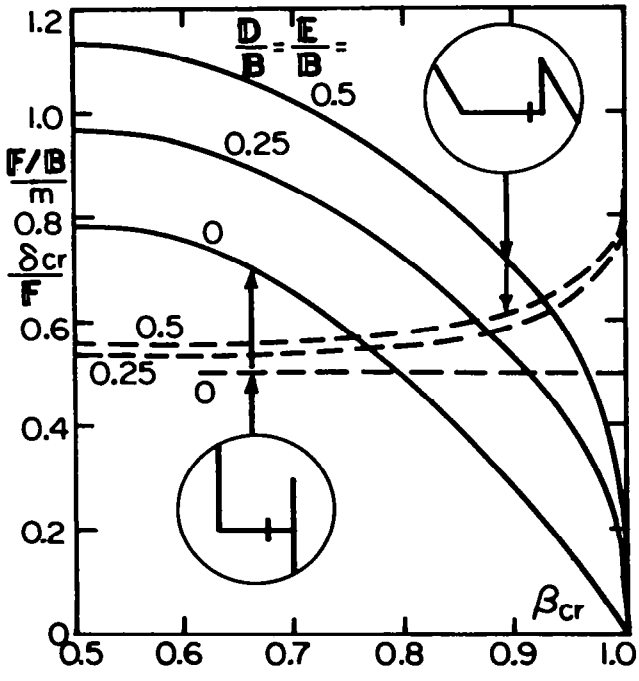

Fig. 3.14. Effect of slant characteristic on recovery throttle setting (β_{cr}) and performance rise at recovery (δ_{cr}), shown dashed, for **E** = **D**.

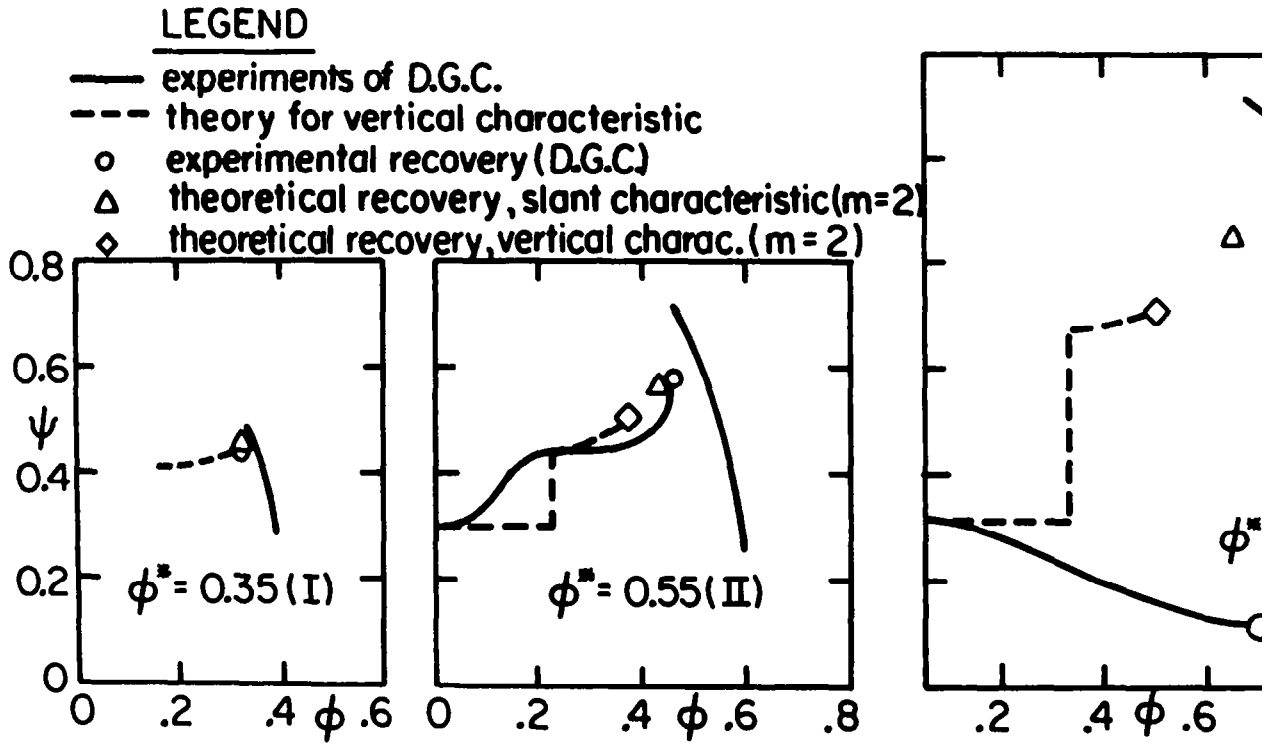

Fig. 3.15. Comparison of theoretical predictions with cases I, II, and IV (50% reac
Greitzer and Cumpsty (D.G.C.), Ref. 3.

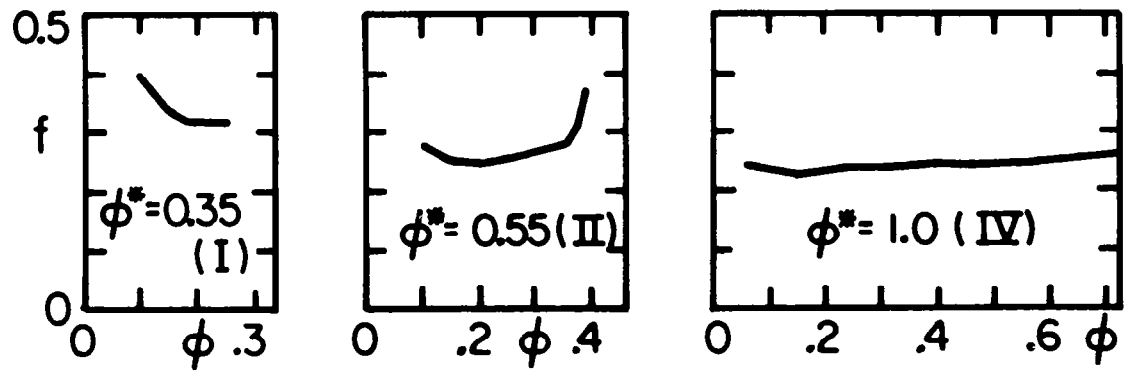

Fig. 3.16. Propagation speed vs flow coefficient for cases I, II, and IV shown on Fig. 3.15. From Fig. 18 of Day's Thesis (Ref. 14). Right margin of each diagram is at recovery value of ϕ.

APPENDIX A

FURTHER ANALYSIS OF THE h-g RELATION

In Part III, the relation $h' = -g$ was used (Eq. (3.6)) in place of the exact potential flow equations for a straight entrance channel. That exact relation is given by Eq. (3.5) or the equivalent Fourier Series:

$$\left.\begin{aligned} \text{If} \quad g &= \sum_{1}^{\infty} (a_n \sin n\theta + b_n \cos n\theta) \\ \text{then} \quad h &= \sum_{1}^{\infty} (a_n \cos n\theta - b_n \sin n\theta) \end{aligned}\right\} . \tag{A1}$$

In Part III, Fig. 3.2 compares $h' = -g$ and Eq. (3.5) for a step-function form of $g(\theta)$. While the result is quite good generally, the simpler form fails near the jumps. Of course, if $g(\theta)$ is harmonic, then $h' = -g$ is exact.

More recently, an improved relation was studied:

$$h' = -Ag + Bg''. \tag{A2}$$

In effect, Part III assumed $A = 1$, $B = 0$. Now we ask whether there might be better choices of A and B. Substituting Eqs. (A1), we find

$$\left.\begin{aligned} h' &= -\sum_{1}^{\infty} (n)(a_n \sin n\theta + b_n \cos n\theta) \\ -Ag + Bg'' &= -\sum_{1}^{\infty} (A + Bn^2)(a_n \sin n\theta + b_n \cos n\theta) \end{aligned}\right\} . \tag{A3}$$

Apparently, the harmonic terms of these two series are identical, and we can match two sets of coefficients, satisfying Eq. (A2) to that extent.

If only first and second harmonics are matched ($n = 1, 2$), then Eqs. (A3) give

$$A = 2/3; \quad B = 1/3 \tag{A4}$$

while if only first and third are matched,

$$A = 3/4; \quad B = 1/4. \tag{A5}$$

Thus, we infer that the best choices of A would typically be a bit less than 1, and B should be quite small.

Recalling Fig. 3.2, we see that a choice like Eq. (A5) for the step-wave would be equivalent to lowering the slope of $h(\theta)$ and adding a $\delta(\theta)$ function at the jumps; this would be a plausible improvement.

Part II provides certain exact solutions of Eq. (A1). They are (Eqs. (2.6a,b))

$$h_0 + ig_0 \equiv \frac{e^{i\theta}}{1 + \eta e^{i\theta}} \tag{A6}$$

$$h_1 + ig_1 \equiv \frac{ie^{i\theta}}{1 + \eta e^{i\theta}} \tag{A7}$$

where η is an arbitrary parameter denoting departure from harmonic shape. Fig. A1 shows the exact values of h_0' and h_1' gotten by differentiating Eqs. (A6,7), for a particular choice, $\eta = 0.4$.

The exact solutions are contrasted with applications of Eq. (A2) for certain A, B combinations. It appears that A = 0.75, B = 0.25 is best. These comparisons are repeated for a more extreme choice of $\eta = 0.7$, and are shown on Fig. A2. In this case, A = 0.85, B = 0.15 seems best. We conclude that Eq. (A2) should represent Eqs. (A1) quite accurately, with A chosen in the range 0.75-0.85 and B in the range 0.25-0.15.

Of course, changing the h-g relation will modify Eq. (3.10). The required change is trivial, however. Define a new variable z,

$$g \equiv -z'; \quad h \equiv Az - Bz''. \tag{A8}$$

Then, Eq. (3.3) becomes

$$(\lambda - Bmf)gg'(z) + Amfz + G(g) - \delta = 0 \tag{A9}$$

instead of Eq. (3.10), and

$$d\theta = -dz/g; \quad \oint zdz/g = 0. \tag{A10}$$

Thus, limit cycles in g,z space may be found just as they were found in g,h space in Part III, with λ replaced by λ - Bmf and mf replaced by Amf. For example, recovery will occur not at f = 1/2, but at a slightly lower value of f:

$$f = \frac{1/2}{1 + Bma} \quad . \tag{A11}$$

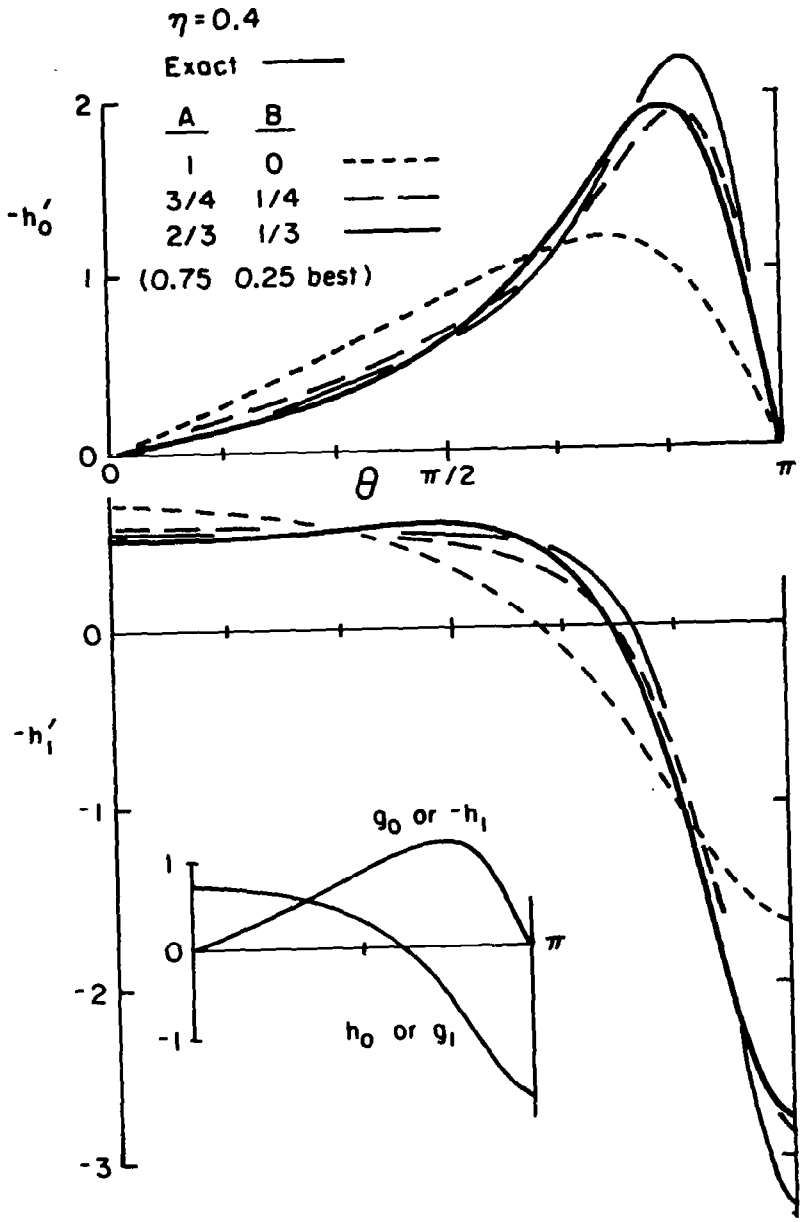

Fig. A1. Evaluation of h-g relations by use of exact solutions, Eqs. (2.6), for moderate nonlinearity, $\eta = 0.4$.

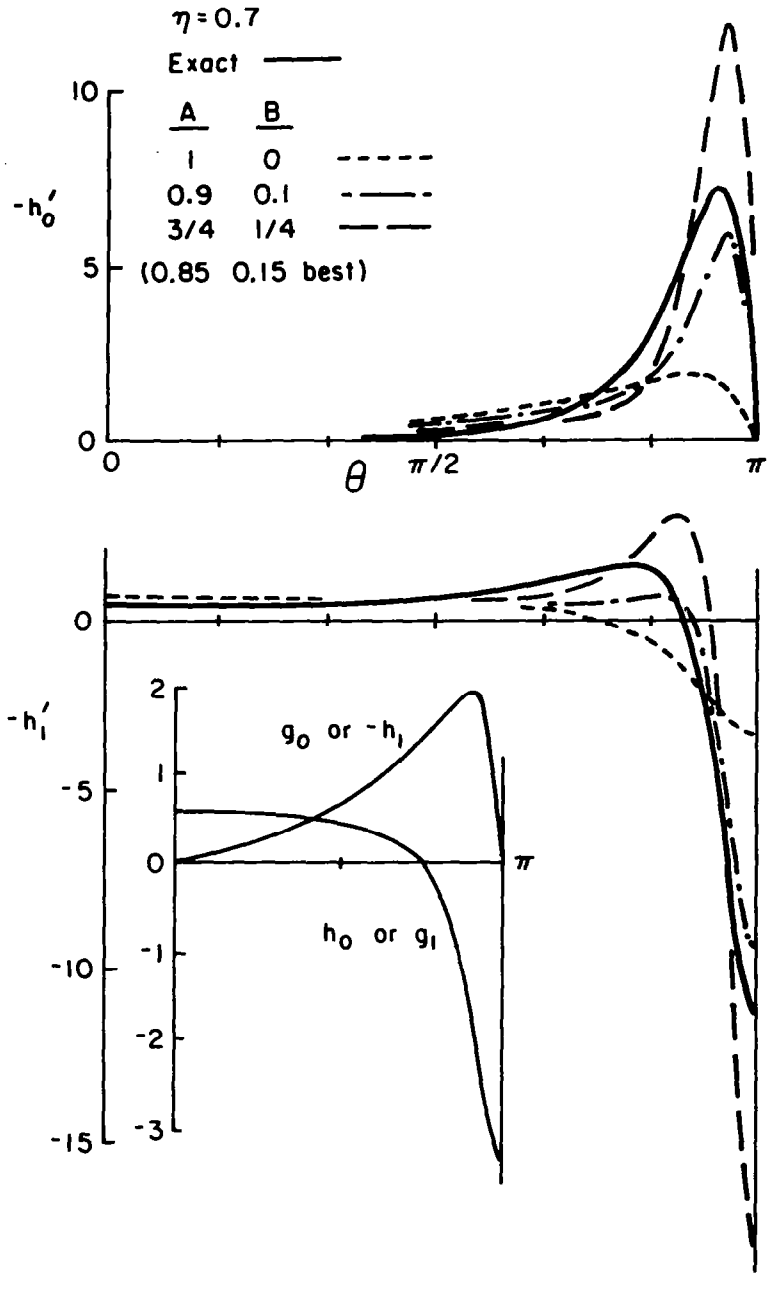

Fig. A2. Evaluation of h-g relations for extreme nonlinearity, $\eta = 0.7$.

APPENDIX B

DETAILED BALANCING AT RECOVERY

In considering the "recovery" results, one is struck by the prediction (borne out be experiment) of sudden jumps of flow coefficient at stall-zone boundaries, and one may wonder how this is possible. The following argument seems to explain the matter.

Beginning with Eq. (3.3), and assuming $h' = -g$, we may write

$$\sigma h'' + mfh + G(-h') + \delta = 0 \qquad \text{(B1)}$$

where $\lambda \sim (2UN\tau/D)(1/2 - f)$ represents the "mass" of an oscillator, mf the "spring constant," and $G(-h') + \delta$ the "dashpot."

We know that recovery is associated with $\lambda = 0$, or, we may say, vanishing oscillator "mass." Certainly, a massless oscillator can undergo a jump-like displacement such as we wish to explain. In our problem, vanishing mass evidently means either vanishing τ or f equal to 1/2. The first possibility is to be rejected as physically untrue; there is always flow inertia in blade passages.

What happens when $f \to 1/2$? Referring to Fig. 1.3, and Eq. (1.3), we see that (for the assumed 50% reaction) when $f = 1/2$, the acceleration ϕ is equal and opposite in rotor and stator blade passages. Specifically, a pressure drop is required in the stator to accelerate the fluid there, and an equal pressure rise is required to decelerate fluid in the rotor. These pressure changes will each be (theoretically) infinite for a step-change of $g(\theta)$, but they will cancel for a stage. Thus, a kind of "detailed balancing" applies to inertial effects in each compressor stage. This result shows an important respect in which single-row and multistage rotating stall must be profoundly different. Cumpsty and Greitzer (9) give another expression of the foregoing idea.

It would be interesting to monitor the row-by-row pressure changes experimentally, to verify the balancing process just described.

APPENDIX C

FURTHER "RECOVERY" RESULTS

A more complete version of Fig. 3.14 may be made by application of Eqs. (3.20,21). Fig. (C1) shows the results when **D** and **E** are not necessarily equal. Clearly, unstalled slope is more important than the reverse-flow slope over most of the range of β. The corresponding results for δ (Eq. (21)) give the same conclusion; they are shown in Fig. (C2). Fig. (C3) shows certain profiles of $g(\theta)$ at recovery.

The recovery analysis is independent of the shape of the characteristic between its extrema. This fact is emphasized in Fig. C4, which shows the recovery points relative to the extrema in a few cases. The displacement is to be measured from the minimum point, in the recovery limit. This result suggests that the rotating-stall-free characteristic is not very important, if we are chiefly concerned with recovery itself rather than approach to recovery.

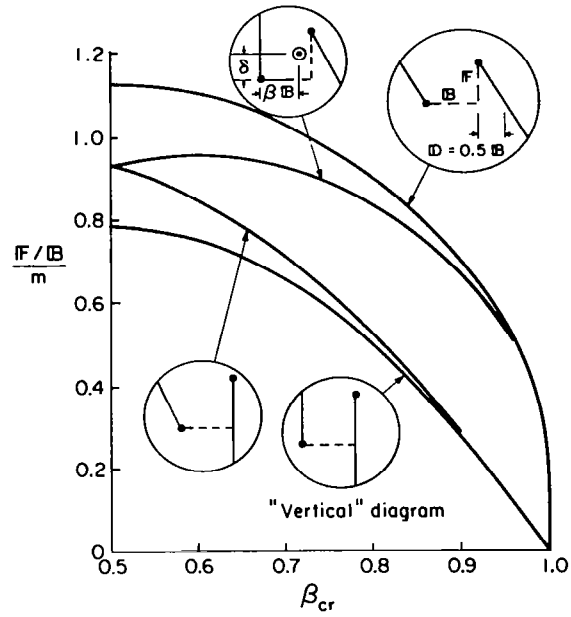

Fig. C1. Recovery requirements, as they depend on slant features of characteristic.

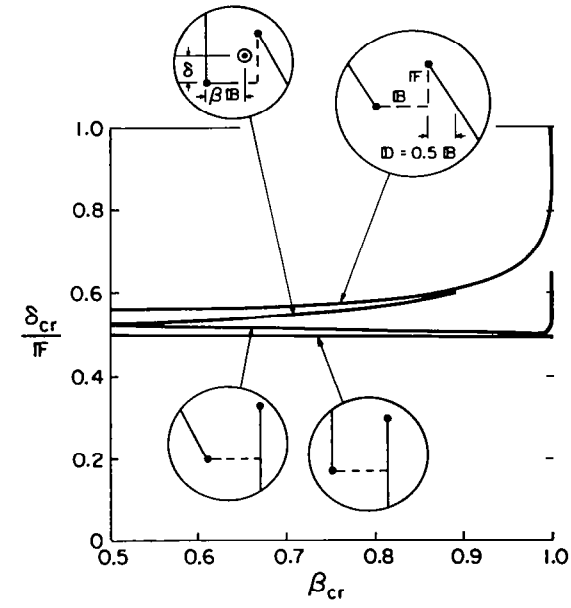

Fig. C2. Average performance increment at recovery, as it depends on slant features of characteristic.

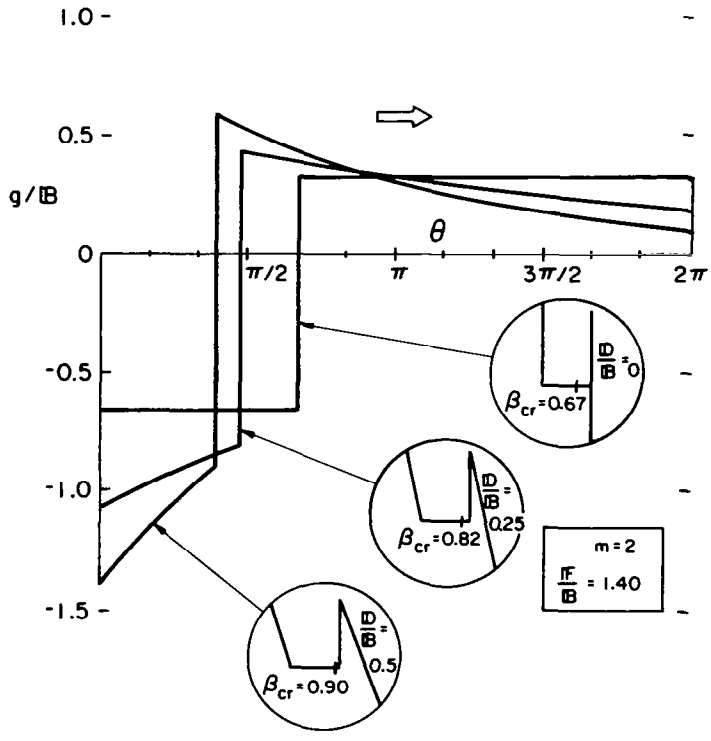

Fig. C3. Recovery profiles of axial velocity vs θ, as they depend on slant features of characteristic.

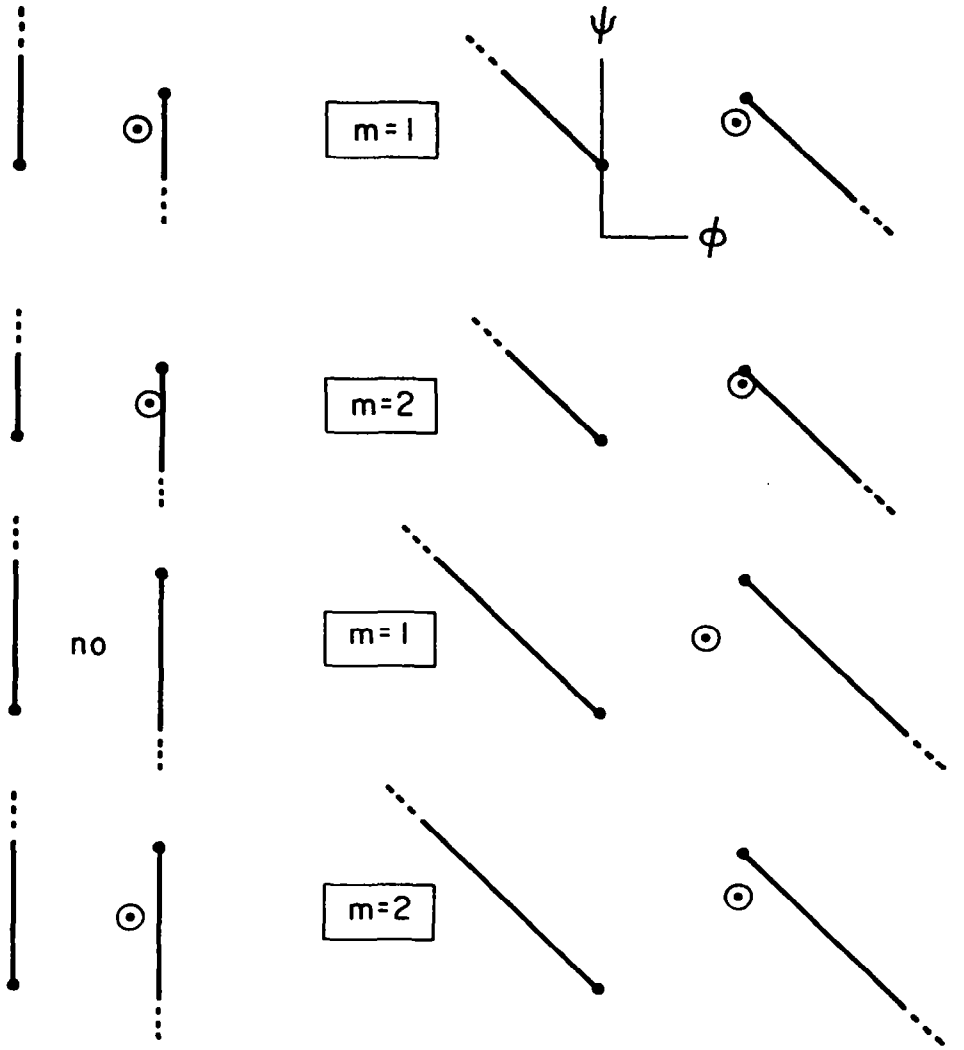

Fig. C4. Recovery point locations (circles points), depending on locations of maximum and minimum points, and slants, of characteristic, for two values of external lag coefficient (m).

APPENDIX D

WEDGE-LIKE ENTRANCE FLOW

If the entrance duct is straight, and a harmonic wave of axial velocity occurs,

$$v = c \sin \theta \tag{D1}$$

then, according to Eq. (1.19),

$$u = c \cos \theta \tag{D2}$$

and we may ask if a different shape would produce a different, perhaps smaller, value of u in response to an imposed v. If so, the important parameter m would be reduced, and rotating stall would be inhibited from occurring.

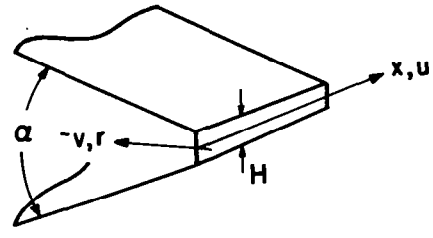

To illustrate this idea, we consider a convergent, straight-sided entrance, as sketched. The shape is two dimensional, and the v velocity varies in the third dimension x, or θ, where $x \equiv (1/2)D\theta$.

We imagine the flow to be axisymmetric and irrotational, so that a velocity potential satisfies

$$\tilde{\phi}_{rr} + \frac{1}{r}\tilde{\phi}_r + \tilde{\phi}_{xx} = 0. \tag{D3}$$

A disturbance at the compressor entrance, where $\alpha r = H$, is assumed:

$$\tilde{\phi} = cT(\zeta)\sin\theta; \quad r \equiv \frac{1}{2} D\zeta \tag{D4}$$

whence a Bessel's equation is found:

$$T'' + \frac{1}{\zeta} T' - T = 0$$

which is satisfied by the function $T = K_0(\zeta)$ (vanishing at $\zeta = \infty$), defined by the series

$$K_0 = -(0.5772 + \ln \frac{\zeta}{2})(1 + \frac{1}{4}\zeta^2 + \ldots) + \frac{1}{4}\zeta^2 + \ldots \qquad \text{(D5)}$$

Thus, at the face,

$$\left.\begin{aligned} -v = \tilde{\phi}_r &= \frac{2c}{D} K_0'(\zeta)\sin\theta \\ u = \tilde{\phi}_x &= \frac{2c}{D} K_0(\zeta)\cos\theta \end{aligned}\right\}. \qquad \text{(D6)}$$

If ζ is small there, $K_0' \approx -(1/\zeta)$ and $K_0 \approx -(0.5772 - \ln 2/\zeta)$. Since $r\alpha = H$ (see the sketch), $\zeta/2 = (1/\alpha)(H/D)$, and

$$v \approx (\frac{2c}{D}\frac{1}{\zeta})\sin\theta$$

$$u \approx \frac{2c}{D}(\ln\frac{2}{\zeta} - 0.5772)\cos\theta.$$

Identifying the coefficient of v as c,

$$u \approx c\,(\ln 2/\zeta - 0.5772)\cos\theta \qquad \text{(D7)}$$

which is to be compared with Eq. (D2). With

$$\frac{\zeta}{2} = \frac{1}{\alpha}\frac{H}{D} \qquad \text{(D8)}$$

we see that a large angle α suggests a small induced u, hence a small value of m, and a reduced tendency to rotating stall. Specifically, if $H/D = 1/10$ and $\alpha = 60°$, Eq. (D7) yields

$$u = 0.338\,c\cos\theta \qquad \text{(D9)}$$

which is only one-third of the straight-duct result.

We conclude that convergence of the entrance region could be an effective means of control of rotating stall.

APPENDIX E

IMPLICATIONS OF THEORY FOR FUTURE RESEARCH

Characteristic Free of Rotating Stall

In this report, it has been assumed that a characteristic speed line $\psi_c(\theta)$ is known, which is apart from the existence of rotating stall, and is free of any hysteresis due to throttle-line slope. Of course, this is not normally measured, because, in experiments, rotating stall does occur, and Parts II and III show that there is a substantial average effect of rotating stall to be expected when the amplitude is large. Also, throttle lines are parabolic, in practice. We note that surge theories or theories which combine surge and rotating stall would assume knowledge of $\psi_c(\theta)$.

Two questions arise: (1) How important is it to know ψ_c?, and (2) how might it be measured? On the first question, Part III, as more fully interpreted in Appendix A, shows that for recovery prediction, only the unstalled and reverse flow legs of ψ_c are needed (assuming that minimum pressure rise is at shut-off), and these can be found well enough from experiments in which rotating stall is allowed. Of course, reverse flow is a rather confusing subject in any case. Fortunately, as the cited discussion shows, the details of reverse flow are of slight importance for recovery.

Thus, ψ_c in the deep-stall range of θ is important only for predicting the complete deep-stall rotating-stall performance. One may suspect that it will prove unimportant for the ultimate theory -- engine-recovery prediction.

The foregoing argument emphasizes the input needed from experiment to make a recovery prediction. An experiment intended to check the prediction of recovery may be another matter, however. In the latter case, throttle related hysteresis could spoil the comparison. That is, the throttle line might osculate the speed line before recovery is reached, as indicated in the sketch. Perhaps this is what happens in the $\phi^* = 1.0$ case of Fig. 3.15. Thus, it may be more important to achieve a steep (ideally, vertical) throttle line than to suppress rotating stall.

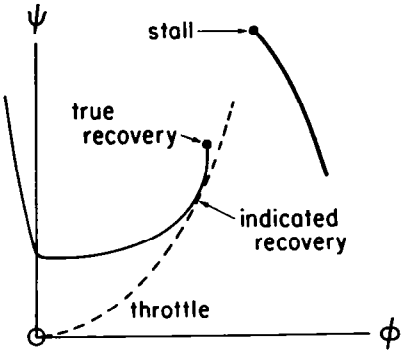

How might ψ_c be measured, free of (a) rotating stall or (b) throttle effect? To accomplish (a), it may be enough to prevent tangential flow velocities in the entrance or exit regions. In principle, honeycomb or vane guidance will work, provided vanes extend all the way to the supply and receiver reservoirs. Probably, some compromise is possible in that regard. A single stage should suffice, provided it is truly representative, because the overall lag in the compressor, which depends on number of stages, is unimportant when rotating stall is to be suppressed anyway.

Another approach might be to add an unstalled compressor in series, closely coupled to the test compressor. However, even the combined characteristic would probably still have a sudden drop where the test compressor stalls, and it seems likely that the combination would still show come rotating stall. For purposes of rotating-stall suppression, the fore and aft honeycomb would seem the most feasible.

To accomblish (b) (elimination of throttle effect), two approaches again seem possible. The most direct method would be to drop the receiver pressure (or raise the supply pressure). That would move the origin of the throttle parabola downward on the diagram, thus steepening the throttle line where it cuts the characteristic at a given flow rate. The range of effect obtainable by this method may be limited. Rather than lowering the throttle origin, it might be better to raise the characteristic by adding a compressor in series, before the throttle. It would not need to be closely-coupled. It should have a high pressure ratio, and, if possible, a rising characteristic as flow is reduced. A centrifugal compressor would be a promising possibility. A difficulty would be that the add-on compressor would have to be at least as powerful as the test machine. To accomplish (b) alone (allowing rotating stall) would mean that the full number of stages would be needed, to get the rotating stall right.

In summary, it would seem possible to find $\psi_c(\theta)$, suppressing rotating stall and throttle-related hysteresis, by adding axial guide vanes extending into slow-flow regions ahead and behind the test compressor, and by adding a second compressor in series betwen the test compressor and throttle. The latter is probably more crucial if the only concern is "recovery."

Entrance/Exit Dynamic Relations

In this report, some rather far-reaching assumptions were made about inlet and exit flows, even though the "external" lag relations are perhaps the most significant determinants of rotating stall. The assumptions were:

(a) Straight entrance duct
(b) Potential flow in entrance
(c) Approximate form of relation between velocity components at entrance
(d) Either straight or "suddenly infinite" exit duct
(e) Inviscid flow in exit
(f) Small-disturbance relation between velocity components in straight exit duct
(g) Constant exit pressure in suddenly infinite exit duct

The foregoing assumptions should be replaced by realistic relations obtained by experiment, with help from theory, treating realistic duct shapes. Velocity and direction, as well as hub and shroud static pressure should be measured close to the front and rear faces, but not too close in terms of individual blade effects. Extremely fast response will be needed to describe stall-zone boundaries which are quite abrupt (but not necessarily square waves).

Such measurements and theories will not only help rotating-stall prediction, but will show the way toward preventive measures, because it is in the entrance and exit flows that suppression of circumferential velocity can best be accomplished.

CFD for Rotating Stall

The comments in the previous paragraphs about the need to measure velocity relationships at the faces of the compressor imply the relevance of CFD. All the assumptions (a)-(g) require new calculations, certainly numerical, to apply theory to the overall compression system. Entrance "goosenecks" are not readily amenable to analysis, nor are the rather short diffusers of current practice.

The Euler equations could be solved in these well-defined regions, subject to various disturbance wave forms for axial velocity. Perhaps, in addition to direct applications, it would prove possible to derive from the numerical results various kernel functions to generalize the velocity relations.

Ultimately, we will be concerned with combined surge and rotating-stall theories. The two-dimensional, third order partial differential equations will surely require CFD treatment ultimately. Probably, the unsteady analysis of flow in blade passages is of less significance than that of entrance and exit regions.

APPENDIX F

SYMBOLS

A	amplitude coefficient of disturbance (Eq. (2.6a) or (3.8))
A_1, A_2	stream-tube stress at entrance to IGV (Fig. 2.3)
a	dimensionless reciprocal time lag, D/(2UNτ)
a_n, b_n	Fourier coefficient of g(θ), Eq. (1.18a)
B	denotes "break" of characteristic (Fig. 2.1)
$\mathbb{B}$	width of characteristic (Fig. 3.4(a))
C	denotes minimum of deep-stall characteristic (Fig. 2.1)
C_p	disturbance of static-pressure rise coefficient across the compressor (Eq. (2.18))
$\mathbb{C}$	rise of deep-stall line (Fig. 3.4(a))
c	constant, App. D
D	mean wheel diameter
$\mathbb{D}$	slant of unstalled leg (Fig. 3.4(a))
$\mathbb{E}$	slant of reverse-flow leg (Fig. 3.4(a))
F	steady pressure rise coefficient in blade passage, Eq. (1.3)
$\mathbb{F}$	height of drop into stall (Fig. 3.4(a))
f	stall propagation-speed coefficient, Eq. (1.11) and Fig. 1.4
G(g)	characteristic function, rotating stall absent (Figs. 3.1 and 3.4(a))
g	axial flow coefficient perturbation in compressor, Eq. (1.4)
H	height of entrance, App. D
h	transverse velocity coefficient perturbation at entrance, Eq. (1.15)
K_I	pressure-rise parameter at IGV entrance, Eq. (1.8)

k	parameter relating actual compressor-row lag to inertia lag of blade passage only
L	depth of row in axial direction, Fig. 1.2(b)
M	denotes maximum of characteristic at stall inception (Fig. 2.1)
m	parameter defining lag tendency outside compressor, Eq. (1.34)
N	number of stages in compressor core
n	wave number, corresponding to number of stall cells
P	pressure coefficient, Eq. (1.24)
p	static pressure
r	distance upstream from apex of wedge, App. D
S	slope of characteristic at "break point" B, Fig. 2.1
U	wheel speed at mean wheel diameter
u	transverse velocity in laboratory frame
V	average axial velocity
v	axial velocity
x	circumferential distance, in stall-zone frame, Eq. (1.5)
y	distance normal to compressor face, in flow direction, Figs. 1.4,5
z	new variable replacing h (Eq. (A8))
α	entrance angle, App. D
β	throttle setting (Fig. 3.4(a))
γ	stagger angle of blades, Fig. 1.2
Δp	pressure recovery at entrance to IGV (Eq. (2.11))
$\Delta\Phi$	difference of flow coefficient at points M and B of Fig. 2.1
δ	performance increase due to rotating stall (Eq. (2.5) or Fig. 3.1)

$\dot{\varepsilon}$	amplitude parameter of disturbance, Eq. (1.19)
ζ	variable, Eq. (D4)
η	nonlinearity parameter of disturbance (Eq. (2.6a))
θ	angular location, in stall-zone frame, Eq. (1.5)
λ	collection of terms analogous to oscillator mass, Eq. (1.39)
ρ	density
σ	normal blade passage width, Fig. 1.2(b)
τ	coefficient of pressure-rise hysteresis, Eq. (1.3)
τ^*	reduced time lag, Eq. (1.45)
Φ	average flow coefficient, V/U
ϕ	flow coefficient, v/U
$\tilde{\phi}$	velocity potential, Eq. (1.13)
Ψ	upstream total to downstream static pressure-rise coefficient existing during operation
ψ_c	compressor characteristic in absence of rotating stall, Fig. 1.1
$\tilde{\psi}$	stream function, Eq. (1.23)

Superscripts

$\cdot$	dot: time derivative
$'$	prime: ordinary differentiation
$\hat{}$	caret: transformation defined by Eq. (3.11)
$\hat{\hat{}}$	double caret: after change of scale so that width of characteristic is 1

Subscripts

cr	critical or recovery value
d	design conditions
e	at compressor exit
IV	inlet guide vane
OV	outlet guide vane
m	amplitude of axial velocity disturbance
mm	conditions when axial velocity disturbance amplitude has its largest permitted value
s	far downstream static conditions
T	far upstream total conditions
v	combined inlet and outlet guide vanes
0	just ahead of compressor entrance
∞	far upstream static conditions

REFERENCES

1. Greitzer, E. M., "Review--Axial Compressor Stall Phenomena," ASME Journal of Fluids Engineering, Vol. 102, June 1980, pp. 134-151.
2. Day, I. J. and Cumpsty, N. A., "The Measurement and Interpretation of Flow within Rotating Stall Cells in Axial Compressors," Journal of Mechanical Engineering Sciences, Vol. 20, 1978, pp. 101-114.
3. Day, I. J., Greitzer, E. M., and Cumpsty, N. A., "Prediction of Compressor Performance in Rotating Stall," ASME Journal of Engineering for Power, Vol. 100, Jan. 1978, pp. 1-14.
4. Emmons, H. W., Pearson, C. E., and Grant, H. P., "Compressor Surge and Stall Propagation," ASME Transactions, Vol. 27, Apr. 1955, pp. 455-469.
5. Graham, R. W., and Guentert, E. C., "Compressor Stall and Blade Vibration," Chapter XI in Aerodynamic Design of Axial-Flow Compressors, NASA SP-36, 1965.
6. Sears, W. R., "Rotating Stall in Axial-Flow Compressors," Zeitschrift fur Angewandte Mathematik und Physik, Vol. 6, No. 6, 1955, pp. 429-455.
7. Marble, F. E., "Propagation of Stall in a Compressor Blade Row," Journal of the Aeronautical Sciences, Vol. 22, 1955, pp. 541-554.
8. Stenning, A. H., Kriebel, A. R., and Montgomery, S. R., "Stall Propagation in Axial-Flow Compressors," NACA TN 3580, 1956.
9. Cumpsty, N. A., and Greitzer, E. M., "A Simple Model for Compressor Stall-Cell Propagation," ASME Paper 81-GT-73, 1981.
10. Stoker, J. J., Nonlinear Vibrations in Mechanical and Electrical Systems, Interscience, New York (1970), Chapter V.
11. Moore, F. K., "Lift Hysteresis at Stall as an Unsteady Boundary-Layer Phenomenon," NACA TN 3571, 1955. Also, Hartunian, R. A., "Research on Rotating Stall in Axial-flow Compressors. Part I. On Lift Hysteresis at Maximum Lift Including Effect of Camber," WADC TR 59-75, January 1959.
12. Takata, H., and Nagano, S., "Nonlinear Analysis of Rotating Stall," ASME Journal of Engineering for Power, October 1972, pp. 279-293
13. Iura, T., and Rannie, W. D., "Experimental Investigations of Propagating Stall in Axial-Flow Compressors," Transactions of the ASME, April 1954, pp. 463-471.
14. Day, I. J., "Axial Compressor Stall," Ph.D. Dissertation, Cambridge University Engineering Department, 1976.

1. Report No. NASA CR-3685	2. Government Accession No.	3. Recipient's Catalog No.
4. Title and Subtitle A Theory of Rotating Stall of Multistage Axial Compressors		5. Report Date July 1983 6. Performing Organization Code
7. Author(s) F. K. Moore		8. Performing Organization Report No. None 10. Work Unit No.
9. Performing Organization Name and Address Cornell University Sibley School of Mechanics and Aerospace Engineering Upsom and Grumman Halls Ithaca, New York 14853		11. Contract or Grant No. IPA 810-626-1 13. Type of Report and Period Covered Contractor Report
12. Sponsoring Agency Name and Address National Aeronautics and Space Administration Washington, D. C. 20546		14. Sponsoring Agency Code 505-40-12 (E-1600)

15. Supplementary Notes

Final report. Project Manager, Calvin L. Ball, Fluid Mechanics and Acoustics Division, NASA Lewis Research Center, Cleveland, Ohio 44135. F. K. Moore on detail from Cornell University, Sibley School of Mechanical and Aerospace Engineering, Ithaca, New York.

16. Abstract

A theoretical analysis was made of rotating stall in axial compressors of many stages, finding conditions for a permanent, straight-through traveling disturbance, with the steady compressor characteristic assumed known, and with simple lag processes ascribed to the flows in the inlet, blade passages, and exit regions. For weak disturbances, predicted stall propagation speeds agree well with experimental results. For a locally-parabolic compressor characteristic, an exact nonlinear solution is found and discussed. For deep stall, the stall-zone boundary is most abrupt at the trailing edge, as expected. When a complete characteristic having unstalling and reverse-flow features is adopted, limit cycles governed by a Liénard's equation are found. Analysis of these cycles yields predictions of recovery from rotating stall; a relaxation oscillation is found at some limiting flow coefficient, above which no solution exists. Recovery is apparently independent of lag processes in the blade passages, but instead depends on the lags originating in the inlet and exit flows, and also on the shape of the given characteristic diagram. Small external lags and tall diagrams favor early recovery. Implications for future research are discussed.

17. Key Words (Suggested by Author(s))	18. Distribution Statement
Rotating stall; Stall; Compressors; Compressor stall; Instabilities	Unclassified - unlimited STAR Category 02

19. Security Classif. (of this report)	20. Security Classif. (of this page)	21. No. of Pages	22. Price*
Unclassified	Unclassified	89	A05

* For sale by the National Technical Information Service, Springfield, Virginia 22161 NASA-Langley, 1983